Progress Report:
Subsidence in California, March 2015 – September 2016

Tom G. Farr, Cathleen E. Jones, Zhen Liu
Jet Propulsion Laboratory
California Institute of Technology

Executive summary

Subsidence caused by groundwater pumping in the Central Valley has been a problem for decades. Over the last few years, interferometric synthetic aperture radar (InSAR) has been used from satellites and aircraft to produce maps of subsidence with sensitivity of fractions of an inch. For this study, we have obtained and analyzed data from the European Space Agency's satellite-borne Sentinel-1A from the period March 2015 – September 2016 and the NASA airborne UAVSAR for the period March 2015 – June 2016, and produced maps of total subsidence from the two data sets. These data add to the earlier data processed from the Japanese PALSAR for 2006 – 2010, Canadian Radarsat-2 for the period May 2014 – January 2015, and UAVSAR for July 2013 - March 2015, for which subsidence measurements were reported previously (Farr et al., 2015). Here we also present results for the South-Central coast of California including Ventura, Oxnard, Santa Barbara and north to the San Joaquin Valley as well as the Santa Clara Valley from colleagues who have processed Sentinel-1A data covering March 2015 – March 2016. As multiple scenes were acquired during these periods, we can also produce time histories of subsidence at selected locations and transects showing how subsidence varies both spatially and temporally. Geographic Information System (GIS) files will be furnished to DWR for further analysis of the 4-dimensional subsidence time-series maps.

The new Sentinel-1A data show the two known main subsidence bowls in the San Joaquin Valley: The larger is centered on Corcoran and extends 60 miles to the NW, affecting the California Aqueduct. For the period May 2015 – September 2016, maximum total subsidence was found to be about 22" near Corcoran. A second bowl is centered on El Nido and is approximately 25 miles in diameter, encompassing most of the East Side Bypass. From May 2015 – September 2016 maximum subsidence totaled about 16" SE of El Nido. A new area, noted in the previous Radarat-2 data near Tranquility about 10 mi SE of Mendota, has intensified in the Sentinel-1A data and subsided about 20" between May 2015 – September 2016. In the Sacramento Valley, Davis and Woodland subsided about 2" from March 2015 – June 2016 and an unusually small intense area of subsidence detected in the previous report near Arbuckle showed a maximum subsidence of about 12". Sierra Valley, an area north of Lake Tahoe not observed in the data acquired for the earlier report showed subsidence of about 6" in an area coincident with lowered water levels in wells.

Data were collected with the NASA UAVSAR airborne platform over the same two swaths previously acquired, and center on the California Aqueduct in order to evaluate subsidence on or near the aqueduct using a high spatial resolution synthetic aperture radar instrument. The northern swath covers the California Aqueduct from the area immediately north of San Luis Reservoir to just south of Kettleman City, and the southern swath covers

the California Aqueduct from due west of Buttonwillow to the Edmonston Pumping Plant. Time series analysis shows subsidence to be highly variable across this extent, as was observed and reported for the earlier UAVSAR data set [Farr et al., 2015]. The fastest subsidence is again observed along the northern stretch of the aqueduct at the Avenal Cut-off Rd. hot spot identified first in summer 2014, where both the amount of subsidence of the aqueduct and the extent of aqueduct experiencing high subsidence has increased substantially. For the period July 2013 – June 2016 subsidence at the center of the subsidence bowl, located in the same place as before (less than half a mile from the aqueduct), is now 27.6", with maximum subsidence of the aqueduct structure equal to 25" and 4.7 miles of the aqueduct experiencing >10" of subsidence. For reference we note that the previously reported values for the period July 2013 - March 2015 were 13" maximum subsidence of the aqueduct and >8" of subsidence along a 1.3 mile stretch of the aqueduct.

Although lower than at the Avenal site, high subsidence continues (1) along the historically subsiding area centered approximately on aqueduct Check 16, and localized near (2) Check 15, (3) Check 19, (4) Check 34, and (5) along the Delta-Mendota Canal at 36°53'N, 120°38'W. Particular effort was made to identify new hot spots immediately adjacent to the aqueduct in both UAVSAR image swaths, particularly small areas of very localized subsidence. Three of these identified, one in the northern UAVSAR swath at 36°51'50"N, 120°46'30"W and the others in the southern UAVSAR swath at 35°20'30"N,119°27'10"W and 34°59''12"N,118°59'30"W. The latter subsidence feature is centered directly on the east side of the aqueduct and experienced a maximum of 6.5" during April 2014 – June 2016.

Introduction

The problem of subsidence

The aquifer system of the southern Central Valley and many other alluvial basins of California has both unconfined and confined parts caused by alternating layers of coarse and fine-grained sediments. Water in the coarse-grained, unconfined or water-table aquifers can be extracted or recharged easily and causes only minor 'elastic' compaction reflected as seasonal subsidence and rebound of water levels and the land surface. Most water wells exploit the deeper confined aquifers, and withdrawal of water from them causes drainage of the fine-grained confining layers called aquitards. Significant amounts of water is available from the aquitards. These, however, drain slowly and compact both elastically and inelastically. In general, if water levels are not drawn too low, when pumping ceases water recharges the aquitards and their structure expands. However, if water levels are drawn too low an irreversible compaction of the fine-grained aquitards occurs. The water cannot recharge the layers, causing permanent subsidence and loss of some groundwater storage capacity (see Galloway et al., 1999 pages 8-13; Bertholdi et al., 1991 for reviews).

Measuring and understanding subsidence as a function of groundwater dynamics will greatly improve management of that important resource. In addition, the effect of subsidence on infrastructure can also be monitored using the remote sensing methodology of synthetic aperture radar interferometry (InSAR) to measure surface deformation using

instruments deployed on satellites or aircraft. The effects of subsidence on infrastructure are varied: Roads can be broken by fissures, pipelines have been exhumed, and the change in slope of the land can alter drainage patterns. This last effect has been observed in natural waterways (a reach of the San Joaquin River slated for restoration work) and water conveyance structures (USBR's Delta-Mendota Canal, DWR's California Aqueduct, local agency irrigation canals) where canal lining raises and other remedial measures have been necessary. Areas of low relief that have subsided are also subject to flooding.

How InSAR works

Key points:

1) InSAR measures subsidence relative to a location chosen during processing.
2) InSAR measures subsidence relative to the first image date in a series.
3) Radar measurements from different instruments deployed on multiple satellites cannot be combined interferometrically.
4) However, subsidence measurements may be combined if they overlap in time.

There are 3 main sources of error in the subsidence maps produced by processing InSAR observations into time series of deformation:

Phase unwrapping errors. These manifest as discontinuities or jumps in the deformation measurement between 2 dates. If the jumps are not too serious and don't show up in many other date pairs, then this type of error doesn't usually cause errors in the aggregated time series.

Temporal decorrelation. Small scale changes (at the scale of a few inches to a foot) in the surface between two radar acquisitions effectively scrambles the phase-difference information. Plowing or vegetation waving in the wind are common causes. If the effect is great enough, the affected areas are blanked out. Otherwise, increased noise will be present in slightly decorrelated areas.

Atmospheric water vapor. This is the most serious error source and the one most difficult to deal with. Water vapor causes a delay in the radar signal that looks exactly like surface deformation. The best way to deal with this is to use the fact that changes in water vapor occur over large areas and tend to come and go while significant surface deformation is usually more local and persistent. Therefore, averaging many pairs of dates will tend to dilute the effect of sporadic water vapor intrusions.

These error sources are treated in more detail in the main body of the report and in the references.

Interferometric synthetic aperture radar (InSAR) is a technique whereby surface change occurring between two radar imaging passes can be measured and mapped to high precision (see Madsen and Zebker, 1998; Massonnet, 1997 for reviews). The ability to map surface deformation of a fraction of an inch over large areas at spatial resolutions of 100 feet or finer has opened up new possibilities for remote monitoring of groundwater resources. Most applications have used satellite radar systems, although airborne systems are also available.

The InSAR technique works by acquiring images from the same viewing geometry at two different times between which a change in the surface position has occurred. The phases of the returning radar waves from the two acquisitions are subtracted to create a phase-difference map, or interferogram, that can be processed to create a map of changes in distance along the line-of-sight direction that are precise to fractions of the radar wavelength (typical wavelengths are 1-10 inches). There are however some noise factors which must be considered, in particular orbital or track position error, atmospheric noise, topography-induced errors, and temporal phase decorrelation. Orbital errors can be handled in the InSAR data processing through re-estimation and topography error is largely removed during post-processing correction. Atmospheric water vapor and other variations in the Earth's troposphere can introduce phase delay artifacts that mimic surface changes and for satellite-borne instruments the ionosphere can also contribute noise. Tropospheric variations are usually dealt with by analyzing many interferometric pairs and averaging (stacking), under the assumption that ground deformation is steady and atmospheric phase is random in time. For time-varying deformation signals, more sophisticated spatiotemporal filtering can be applied during InSAR time series analysis to mitigate the effects of atmospheric noise (Galloway et al., 1998; Lanari et al., 2004; Ozawa and Ueda, 2011; Chaussard et al., 2013). Another problem, especially acute in agricultural areas like the Central Valley, is small-scale surface changes near the scale of the radar wavelength. Crops blowing in the wind or fields plowed between radar image acquisitions can spoil the phase coherence between the two radar images and cause loss of information. This effect can be ameliorated by using a longer wavelength and selecting interferometric pairs that have small orbital track (baseline) separations and temporal differences.

After many pairs of radar images over an area have been processed into interferograms, they can be further analyzed to create a time series of surface deformation. This is done by an InSAR time series inversion algorithm called the Small Baseline Subset (SBAS) method (Berardino et al., 2002; Sansosti et al., 2010). SBAS makes use of interferometric pairs that have small spatial baselines and short temporal separations. The time series is constructed pixel by pixel and requires no assumptions on the continuity or stability of phase in time. Proper choice of the reference location is needed in order to tie together the relative InSAR measurements into a consistent reference frame. The reference location (or pixel) is usually chosen at a place that is stable compared to the deformation of interest based on *in situ* geodetic measurements or *a priori* information.

The InSAR time series analysis produces a history of line-of-sight (LOS) surface displacements similar to GPS time series observations but with much higher spatial resolution. InSAR time series recover both long-term mean LOS velocities and the time varying components, while at the same time isolating atmospheric delays (as well as surface deformation) into the respective SAR image epochs (e.g., Lanari et al., 2004). This technique has been applied successfully for imaging non-steady-state deformation at volcanoes (Lundgren et al., 2004), deforming plate boundaries (Lundgren et al., 2009), and aquifer dynamics (Farr et al., 2015; Farr, 2011; Lanari et al., 2004). After the initial time series inversion, temporal and spatial filtering can be applied to further suppress turbulent atmospheric noise and smooth the deformation time series. The satellite results shown here have been averaged to 300' pixels in order to reduce the random errors. Since

atmospheric noise is spatially correlated but temporally uncorrelated, its net effect on the InSAR time series is usually negligible. The estimated measurement precision for InSAR time series is generally a small fraction of a wavelength, depending on the InSAR acquisitions and noise levels (Galloway et al., 1998; Ozawa and Ueda, 2011; Chaussard et al., 2013). In the case of the Sentinel-1A measurements used for the subsidence measurement, uncertainties associated with the vertical displacement (subsidence/uplift) measurements were determined to be less than 1" and usually less than 0.5". For the UAVSAR-derived subsidence measurements accuracies of 0.25"-1" are obtained. These uncertainties cover random errors, but do not include systematic errors related to choice of reference location, unwrapping errors, spatially correlated residual atmosphere noise, or uncorrected ionosphere errors.

A final step in post-processing is to project the LOS measurements to the vertical direction under the assumption that there is no significant horizontal surface movement gradient and all of the measured deformation comes from subsidence/uplift. This allows measurements from multiple satellites with different imaging geometries to be compared with each other. The results can also be compared with vertical surface change measured with GPS and traditional surveying methods.

Several groups have made studies of the effects of groundwater withdrawal and recharge on InSAR measurements of deformation of the Earth's surface (Reeves et al., 2011; Calderhead et al., 2011; Lu and Danskin, 2001; Amelung et al., 1999). Preliminary evaluations of InSAR applications to groundwater monitoring in the western United States have been made over the last few years for Los Angeles (Bawden et al., 2001), the Antelope Valley (Galloway et al., 1998), Las Vegas (Hoffmann et al., 2001; Bell et al., 2008), the Santa Clara Valley (Sneed et al., 2003), the Coachella Valley (Sneed and Brandt, 2007), and the southern Central Valley (Farr and Liu, 2015; Farr, 2011; Sneed et al., 2013; Borchers and Carpenter, 2014).

A number of satellite systems have been flown over the years to provide InSAR data (Table 1). Note that while the satellites span only a few years each, they overlap in time allowing their time series to be compared. That is a focus of ongoing research in our group at JPL. For the previous report (Farr et al., 2015), PALSAR images spanning the period June 2007 – December 2010 and Radarsat-2 images for the period May 2014 – January 2015 were processed to two independent time series. This report uses Sentinel-1A to cover May 2015 – August 2016 and later and is continuing to add new data to the time series. Details of the data used are listed in the Appendix. Further work under this task will fill the gap between the PALSAR and Radarsat-2 results using Radarsat-1 data.

Satellite	dates	resolution (m)	swath (km)	incidence angles	minimum revisit (days)	band*/pol
ERS 1,2	1991-2010	25	100	25°	35	CVV
Envisat	2002-2010	25	100	15-45°	35	CVV, CHH
PALSAR	2006-2011	10-100	40-350	10-60°	46	L-quad
Radarsat 1	1995-2013	10-100	45-500	20-49°	24	CHH
Radarsat 2	2008-	3-100	25-500	10-60°	24	C-quad
TerraSAR-X	2007-	1-16	5-100	15-60°	11	X-quad
Cosmo-Skymed	2007-	1-100	10-200	20-60°	<1	X-quad
PALSAR-2	2014-	3-60	50-350	8-70°	14	L-quad
Sentinel-1A	2014-	20	250	30-45°	12	C-dual
NISAR	2020?	35	350	15-60°	12	L-quad

* wavelengths: X ~ 3 cm, C ~ 5 cm, L ~ 25 cm

Table 1. Past, present, and future radar satellites. The resolution specified is the values for the instrument prior to spatial averaging.

UAVSAR, which is an L-band SAR flown on a Gulfstream-3 aircraft, has a much higher signal-to-noise ratio than satellite SARs, usually achieving a factor of 100 increase in signal through the use of a high-power instrument transmitting from 41,000 ft. altitude rather than from Earth orbit. It also has higher spatial resolution than the satellite SARs, with <6' instrument ground resolution, which allows significantly higher resolution than satellite SARs when accounting for the spatial averaging that is done to reduce the phase noise. The reduction in phase noise means that deformation measurement accuracy is increased and temporal decorrelation is reduced. The practical outcome is that a larger proportion of a UAVSAR scene will produce useful measurements. Previous InSAR results from UAVSAR include measurements of fault slip in California (Donnellan et al., 2014), landslides along the San Andreas fault (Scheingross et al., 2013), and sinkhole precursory ground movement in Louisiana (Jones and Blom, 2014).

The UAVSAR data analysis methods used in this work are based on procedures developed to monitor the levees in the Sacramento-San Joaquin Delta using the instrument (Jones et al., 2012; 2015; Sharma et al., 2015). Unlike in the Central Valley, groundwater pumping is not a problem in the Sacramento-San Joaquin Delta. However, subsidence from aerobic oxidation of the soil and compaction of the soil from pumping to remove water from the upper layers of the soil is common throughout the area (Deverel and Leighton, 2010). UAVSAR data processing initially followed similar steps to those used for the satellite data. Low coherence areas for which the subsidence could not be determined accurately were eliminated from the analysis by masking out pixels with that were not correctly phase unwrapped in at least 80% of the interferograms. This masking step eliminated most open water and land areas that experienced high and persistent temporal decorrelation. A temporal filter of width 1 month was applied to smooth the results; this value was chosen to be sufficiently short that we are able to resolve when subsidence rates changed during

2014. Tropospheric phase noise was estimated using the open source Toolbox for Reducing Atmospheric InSAR Noise (TRAIN) (Bekaert et al., 2015).

After performing the time series InSAR analysis, further processing was carried out to improve subsidence estimation in low coherence areas. Pixels were classified based upon their average coherence, and adaptive spatial filtering was applied such that low coherence areas were averaged with nearby same-class pixels to reduce noise, and high coherence pixels were not averaged at all. Uncertainties in the derived subsidence values were obtained through a Jacknife resampling procedure whereby the SBAS processing was run on the stack with data from a single acquisition removed, repeated with removal of each acquisition date in the series. This procedure estimates the combined effect of random errors and systematic errors associated with a single acquisition. The uncertainties in the cumulative subsidence derived from UAVSAR InSAR are in the range of 0.25" to 1.0" across most of the imaged area. Estimates for each pixel are included in the GIS products provided to DWR, and shown in plots in an appendix to this document.

San Joaquin Valley Subsidence

Maps of subsidence in the San Joaquin Valley were made for the period May 7, 2015 – September 10, 2016 (Fig. 1). Two main subsidence bowls can be seen in the maps of total subsidence: A southern one in the Tulare basin about 25x65 mi. centered on Corcoran and a northern one about 15x25 mi. centered S of the town of El Nido. The maximum total subsidence in the Tulare Basin was about 22" near Corcoran. The maximum subsidence SE of El Nido was approximately 16". These patterns are generally similar to the earlier PALSAR and Radarsat-2 results, but we see continued development of a diffuse area NW of Corcoran with a subsidence of up to 12". Subsidence of over 12" extends W to the California Aqueduct near Avenal; at the aqueduct is a small patch of total subsidence of almost 18" which occurred during two periods: May-Oct. 2015 and Apr.-Aug. 2016 (Fig. 2).

The northern subsidence bowl SE of El Nido subsided about 16" with pockets up to 20". The East Side Bypass runs right through the main part of the subsidence in this area. A relatively new area of subsidence has been recognized near Tranquility about 10 mi SE of Mendota. This was first noted in Radarsat-2 data for late 2014, but has intensified in the meantime. The area is about 7 mi in diameter. Its history of subsidence (Fig. 2) shows it subsided in 2 stages: early May – Oct. 2015 and Apr. – Aug. 2016.

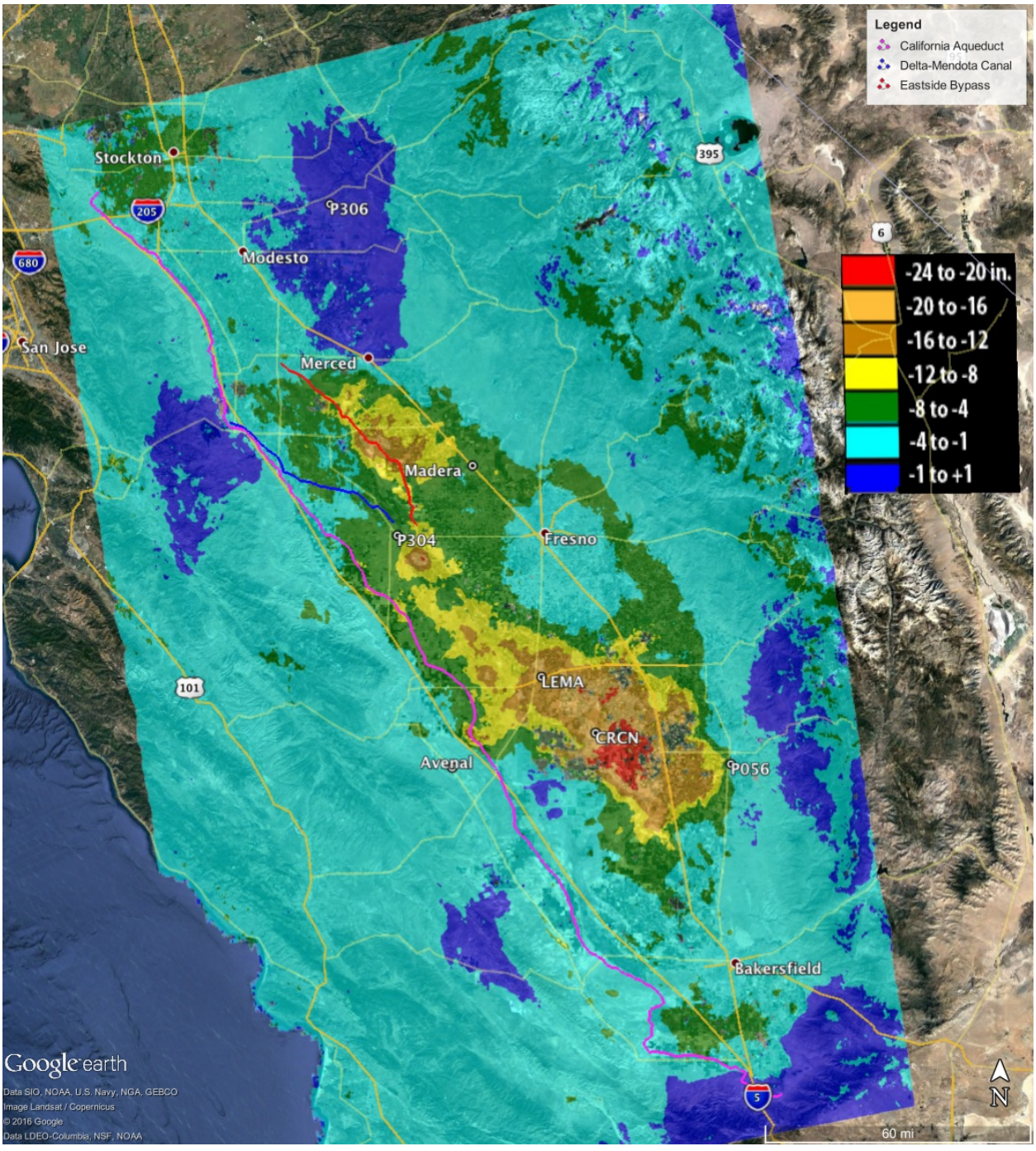

Figure 1. Total subsidence in the San Joaquin Valley for the period May 7, 2015 – Sept. 10, 2016 as measured by ESA's Sentinel-1A and processed at JPL. Two large subsidence bowls are evident centered on Corcoran and SE of El Nido with a small, new feature between them, near Tranquility. An arm of the large Corcoran bowl also extends to the California aqueduct near Avenal.

The deformation histories of a few selected locations in the San Joaquin Valley are plotted in Figure 2. The large maximum subsidence in the Corcoran area is clear and shows virtually no recovery at any time during the period of measurement. The maximum subsidence location near El Nido shows some flattening between Oct. 2015 and Mar. 2016. The relatively new subsidence feature at Tranquility and the history of the aqueduct

feature near Avenal also show a flattening between Oct. 2015 and Mar. 2016, but renewed subsidence after Apr. 2016. There is some suggestion that the subsidence slows starting in Aug. 2016, but as discussed later, this may be an artifact of atmospheric water vapor contamination.

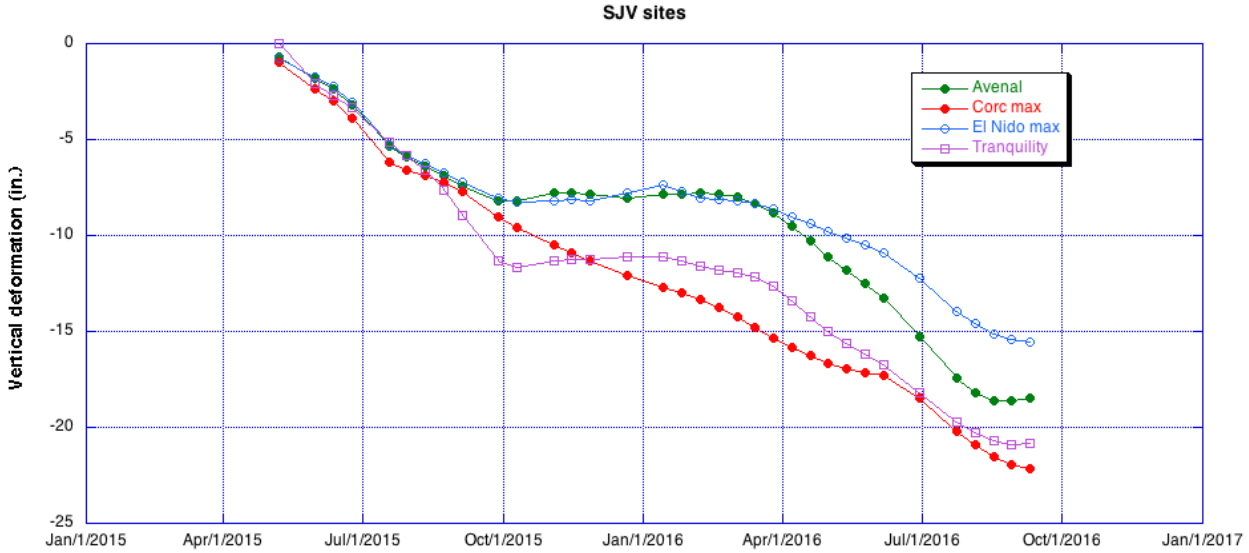

Figure 2. Subsidence histories of a few locations in the San Joaquin Valley. 'Avenal' is located at the maximum subsidence measured near the California aqueduct near the town of Avenal. This was also mapped by UAVSAR (Fig. 8). Corcoran max is located in the maximum subsidence pocket S of Corcoran. El Nido max is located in the pocket SE of El Nido. Tranquility is located at the maximum subsidence 9 mi SE of Mendota, between the two main subsidence bowls.

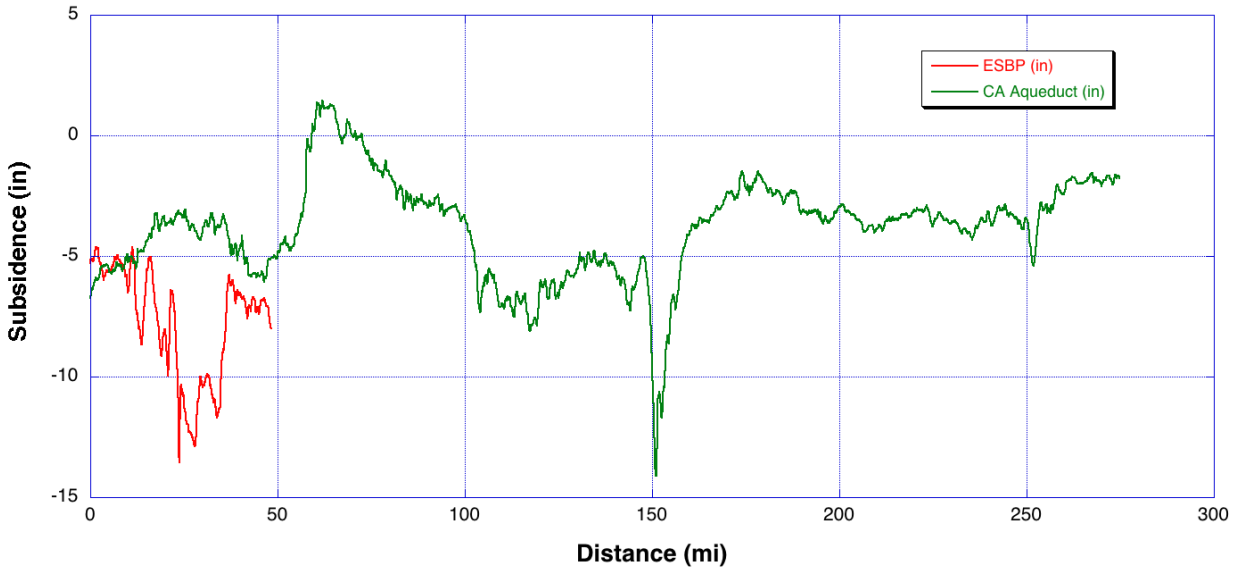

Figure 3. Transects showing total subsidence along the California Aqueduct and the East Side Bypass. The transects extend from N to S and represent total subsidence from May 7, 2015 – May 25, 2016. Note the deep subsidence about midway along the East Side Bypass. That corresponds to the red area on the map (Fig. 1). The sharp pit near mile 150 on the California Aqueduct corresponds to the feature near Avenal and shown in Fig. 2.

The transects shown in Figure 3 give a more detailed picture of the total subsidence measured in the vicinity of the California Aqueduct and the East Side Bypass over the period of measurement. It is clear that the East Side Bypass has suffered significant subsidence, concentrated in its central area. In contrast, most areas in the vicinity of the California Aqueduct experienced only a few inches of subsidence. The exception is the subsidence concentrated near Avenal and plotted near mile 150. This location was recognized in the previous report. These amounts correspond to averages over the processed pixel (about 300'), not the values on the aqueduct structure itself.

Subsidence histories at specific locations can also be compared with continuous GPS measurements obtained throughout the Central Valley (Fig. 4). Here, we compare our measurements with data from the Plate Boundary Observatory (http://www.unavco.org) and 2 CalTrans sites (http://www.dot.ca.gov/dist6/surveys/CVSRN/index.htm). Note that large subsidence signals show up very reliably in the InSAR time series, but that there are excursions from the GPS time series. As discussed earlier, these are most likely due to water vapor variations in the lower atmosphere which cause phase delays of the radar waves which mimic deformation. It is very difficult to eliminate this effect without precise maps of the water vapor obtained at the same time as the radar observations. Therefore the most practical way to deal with these variations is to acquire observations at many dates and use the fact that the water vapor variations are not correlated from date to date to 'average' out the effects. We expect that as more dates are obtained for California, the time series and subsidence maps will become more consistent.

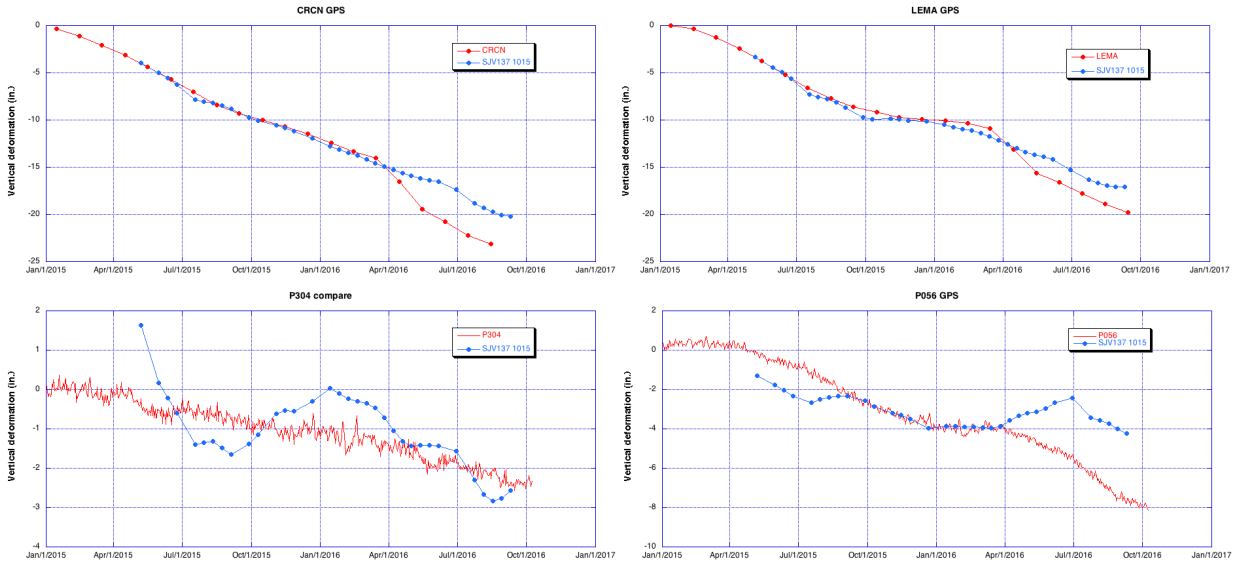

Figure 4. Selected comparisons of GPS vertical time series and InSAR time series at the same locations in the San Joaquin Valley projected to vertical. InSAR time series have been arbitrarily offset vertically for an optimal match to the GPS time series. GPS sites are shown in Figure 1. The upper two plots have the same range of Y values and all plots have the same date range. Note some large deviations, most likely due to water vapor variations affecting the InSAR phase measurements.

UAVSAR Results Along California Aqueduct

Figure 5 shows coverage of the Central Valley by the two UAVSAR flight lines used for monitoring movement in close proximity to the California Aqueduct. The values shown are cumulative for the full time period of measurement, starting in mid-2013 (northern line) or sping-2014 (southern line) and extending through June 2016. A common color scale is used to show that the swath to the north has many locations experiencing significantly greater subsidence than is observed in the southern swath. Overall the trends are similar to what was reported previously (Farr et al., 2015), with higher subsidence in the San Luis Field District section of the aqueduct. However, the amount of subsidence experienced has increased significantly, with 60-100% increases typical in both areas.

Areas showing high subsidence rates, including rates that are anomalous relative to the surrounding area and localized near the aqueduct, are highlighted individually below for line 14511 (Figure 6) and line 13300 (Figure 7). We note that subsidence values measured with UAVSAR InSAR are averaged across a pixel of area ~ 20' x 20', so maximum values measured on the ground could be higher at locations within the pixel.

Figure 6 shows only the northern imaged swath. In this stretch of the aqueduct there is an extended region of subsidence in the center, an area of very high subsidence with a very well-defined locus adjacent to Avenal Cut-off Rd., and several other areas showing high subsidence. Signals typical of well withdrawal are observable away from the aqueduct to the east of the hot spot at Avenal Cut-off Rd. These show up as broader scale subsidence in the satellite image (Figure 1) but can be resolved and localized to identify their source locations with the higher resolution and lower noise of the UAVSAR data.

The highest amounts of subsidence occur at the previously identified localized subsidence bowl located between Huron and Kettleman City directly to the north of Avenal Cut-off Rd. and Check 20, referred to as the Avenal hot spot (Figure 8). This feature has deepened to 27.6" at its maximum and expanded so that the aqueduct has subsidence as much as 25", with the greatest subsidence near the previous maximum subsidence location directly west of the hot-spot center. The area of impact from the hot spot has dramatically increased, with ~4.7 miles of the aqueduct experiencing 10" or greater subsidence since the measurements started in July 2013 and most of that occurring since summer 2014. For reference, the previously reported values for the period July 2013 - March 2015 were 13" maximum subsidence of the aqueduct and >8" of subsidence along a 1.3 mi stretch of the aqueduct. In addition, Figure 8 shows that it is possible that two smaller hot spots are

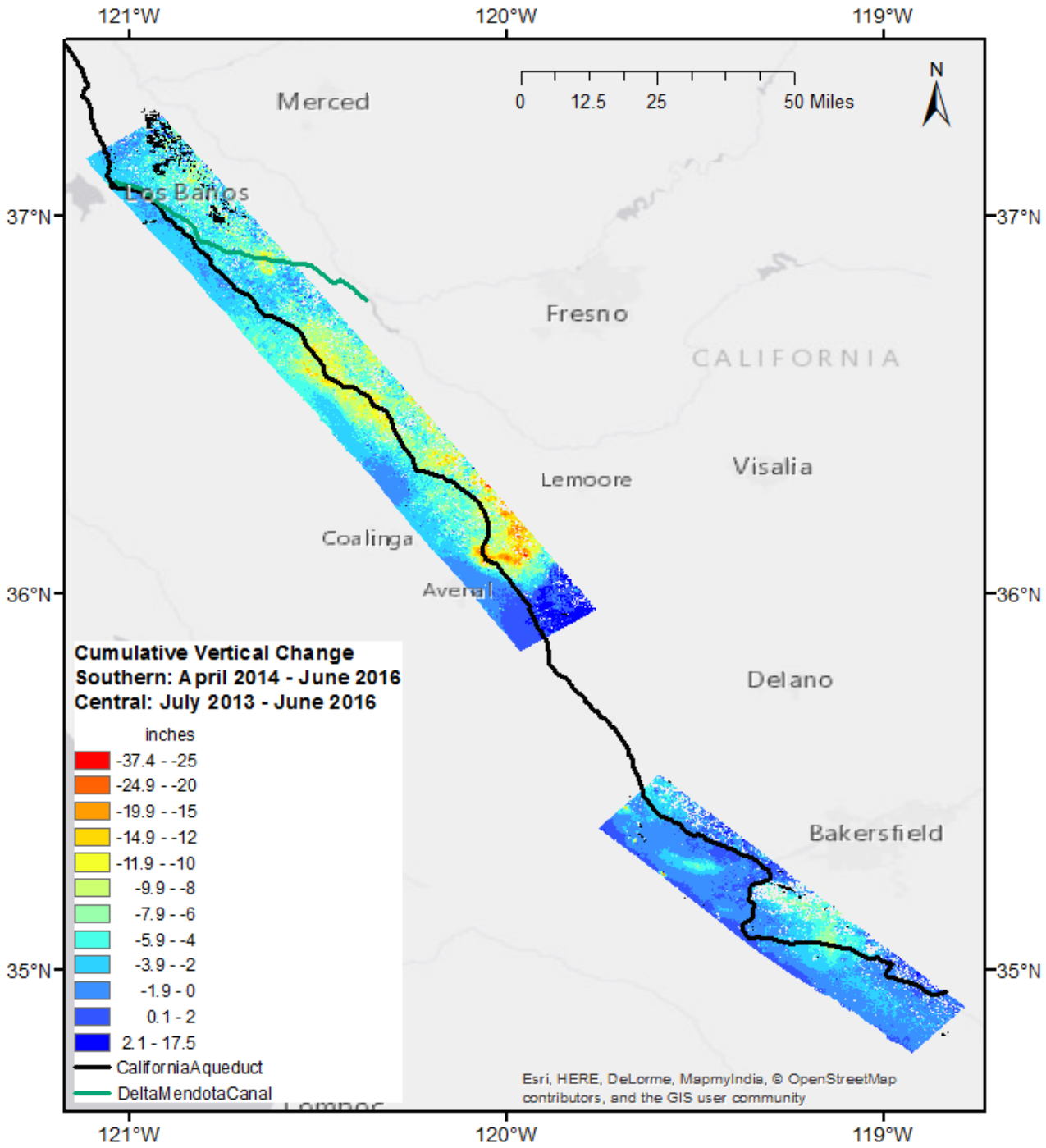

Figure 5. Overview of subsidence measured in the two UAVSAR image swaths covering the California Aqueduct. These swaths were planned specifically to image the California Aqueduct, and therefore miss the large subsidence bowls to the east that are seen in the satellite SAR results. The swath to the south, which covers part of the aqueduct in the San Joaquin Field District, is UAVSAR line 13300 and shows cumulative subsidence between April 2014 and June 2016. The swath to the north, which covers the central section of the California Aqueduct (San Luis Field District), is UAVSAR line 14511 and shows cumulative subsidence between July 2013 and June 2016. Part of the Delta Mendota Canal is included in the northern swath.

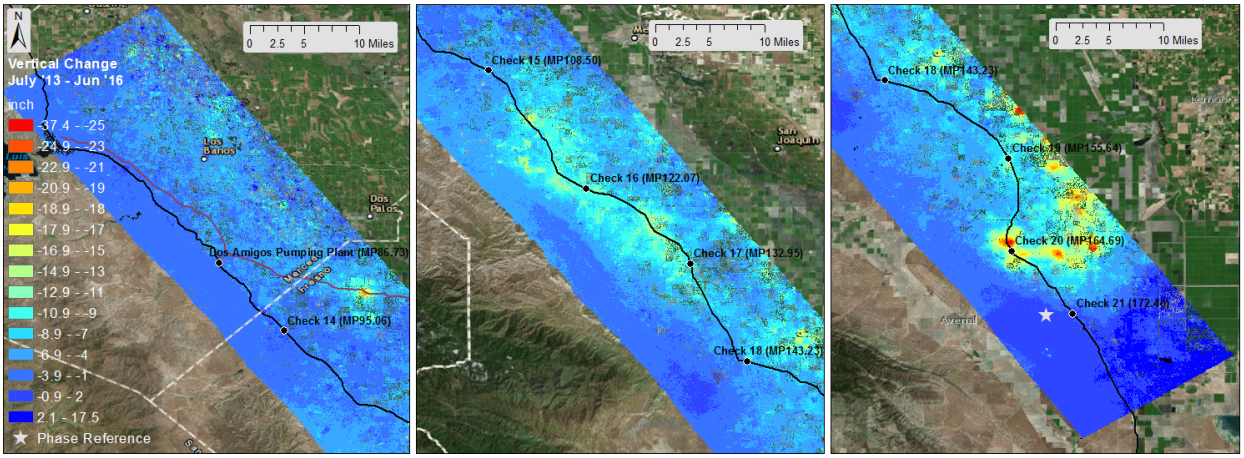

Figure 6. Overview of cumulative subsidence between July 2013 and June 2016 in the northern UAVSAR swath, which covers the part of the California Aqueduct in the San Luis Field District. The swath is split into three images with the northern/center/southern part of the line plotted at left/center/right. The hot spot of subsidence near Avenal Cut-off Rd. has expanded and is now very apparent on the broad-scale map. A second smaller subsidence bowl is developing immediately to the south and other localized bowls are seen to the east. The star indicates the reference location, relative to which subsidence at other locations is measured.

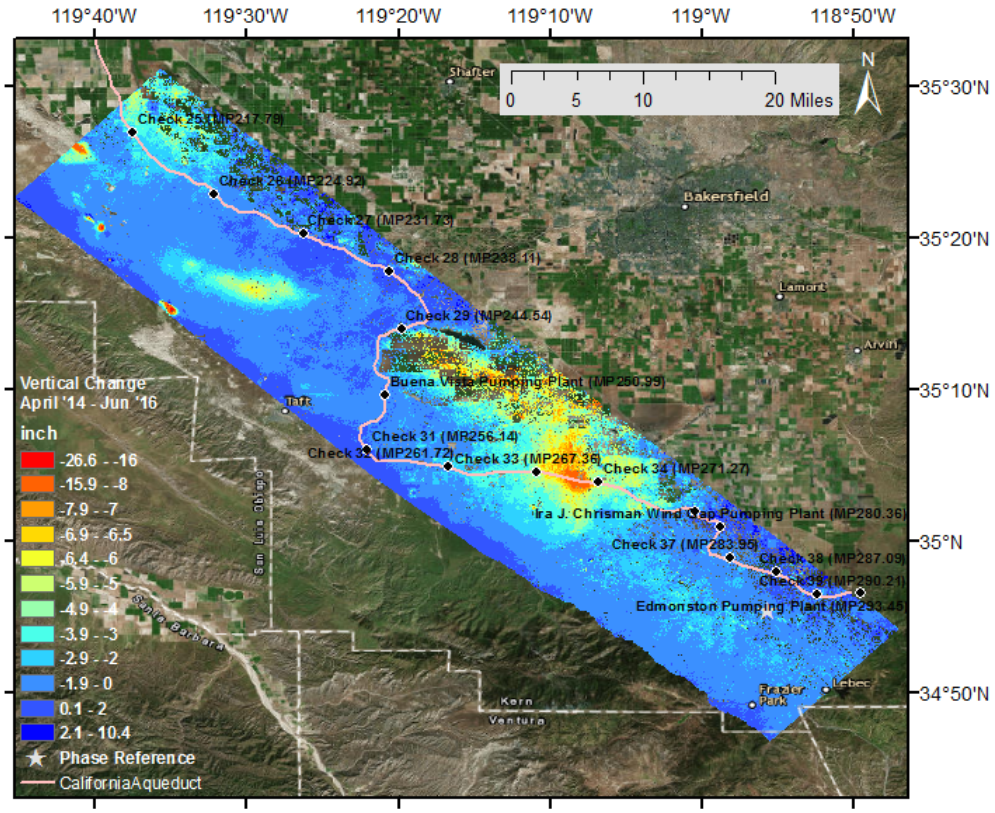

Figure 7. Overview of cumulative subsidence between April 2014 and June 2016 in the southern UAVSAR swath, which covers the part of the California Aqueduct in the San Joaquin Field District. The broad-scale subsidence impacts the aqueduct most significantly between Check 33 and Check 34, and less significantly near the northeast edge of the swath. Localized subsidence/uplift areas to the east are oil fields. The star indicates the reference location, relative to which subsidence at other locations is measured.

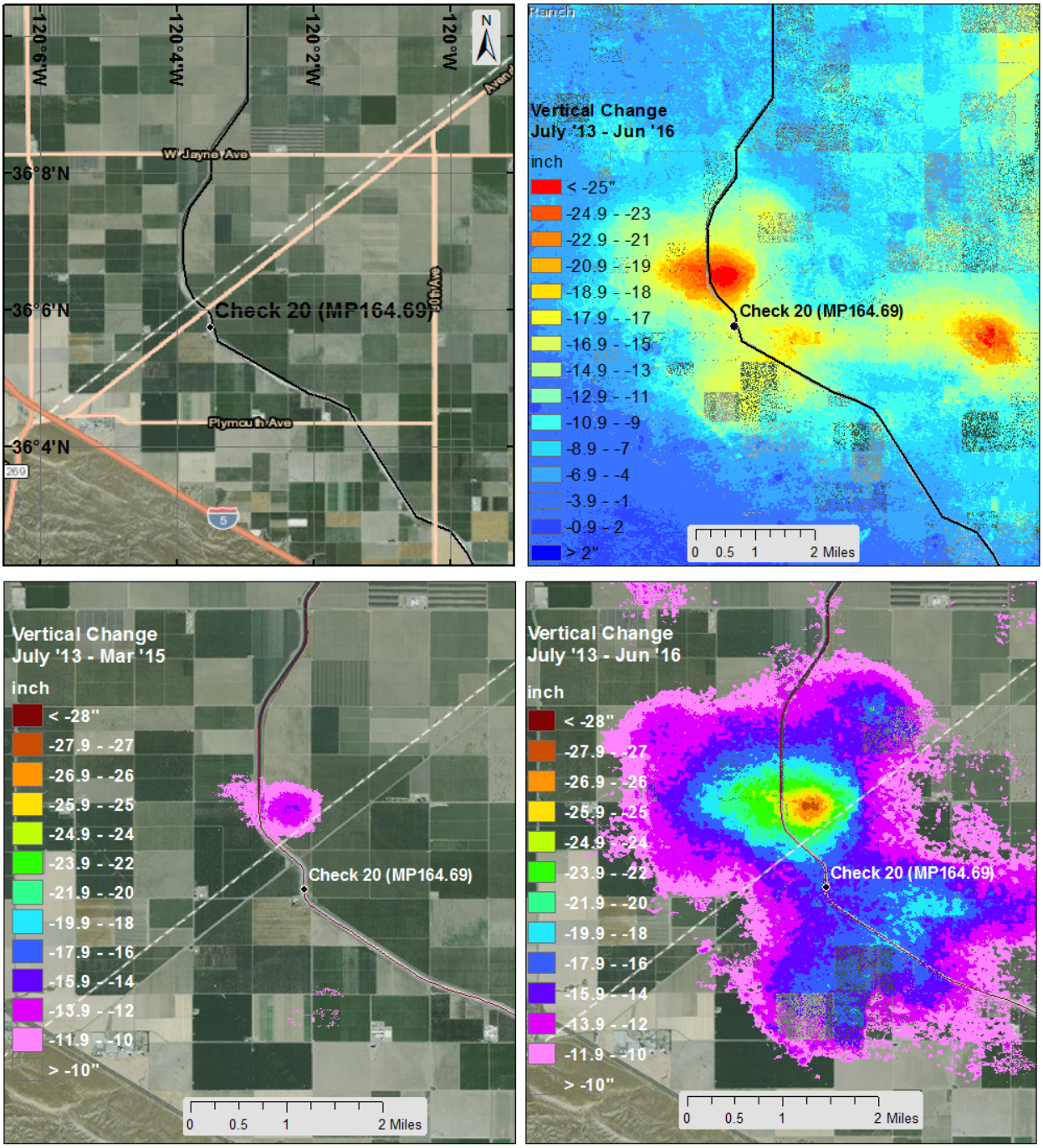

Figure 8. Optical image with latitude/longitude specified (top left) and subsidence map (upper right) showing the subsidence hot spot centered just north of Avenal Cut-off Rd. and <0.5 mi east of the California Aqueduct. Much smaller hot spots are potentially forming centered <1 mi from the aqueduct to the northeast and southeast of the main subsidence bowl. Another large and localized subsidence bowl several miles to the east of the aqueduct has also deepened and expanded (upper right). The bottom two maps show the relative expansion of the subsidence bowl between March 2015 (bottom left) and June 2016 (bottom right). The same color scale is used for both and only areas subsiding >10" are plotted. The aqueduct now shows areas with 25" of subsidence. Approximately 5 miles of the aqueduct has been lowered by >10".

forming centered <1 mi from the aqueduct, one directly to the northeast and the other directly southeast of the main subsidence bowl. Furthermore, another large and localized subsidence bowl several miles to the east of the aqueduct has deepened and expanded since the last reported subsidence in March 2015 (Figure 8, upper right). Because this bowl has similar magnitude to the Avenal hot spot, its area of influence is also likely to expand if pumping continues.

A comparison between results for the Avenal hot spot from Sentinel (Figures 1, 2, and 3) and UAVSAR (Figure 8) for the Avenal area show a similar rate of subsidence. However smaller areas noted below generally don't show up in coarse-resolution satellite data.

Two new localized subsidence features similar in shape to the Avenal hot spot, albeit smaller in magnitude, have been identified. One is located south of San Luis Reservoir and north of Check 14 (36°51'50"N, 120°46'30"W) (Figure 9) and the other south of the Wind Gap Pumping Plant and north of Check 37 (34°59''12"N, 118°59'30"W) (Figure 10). In addition, a small subsidence feature in the shape of an arc north of Check 27 and at the location of a former seep continues to subside (Figure 11).

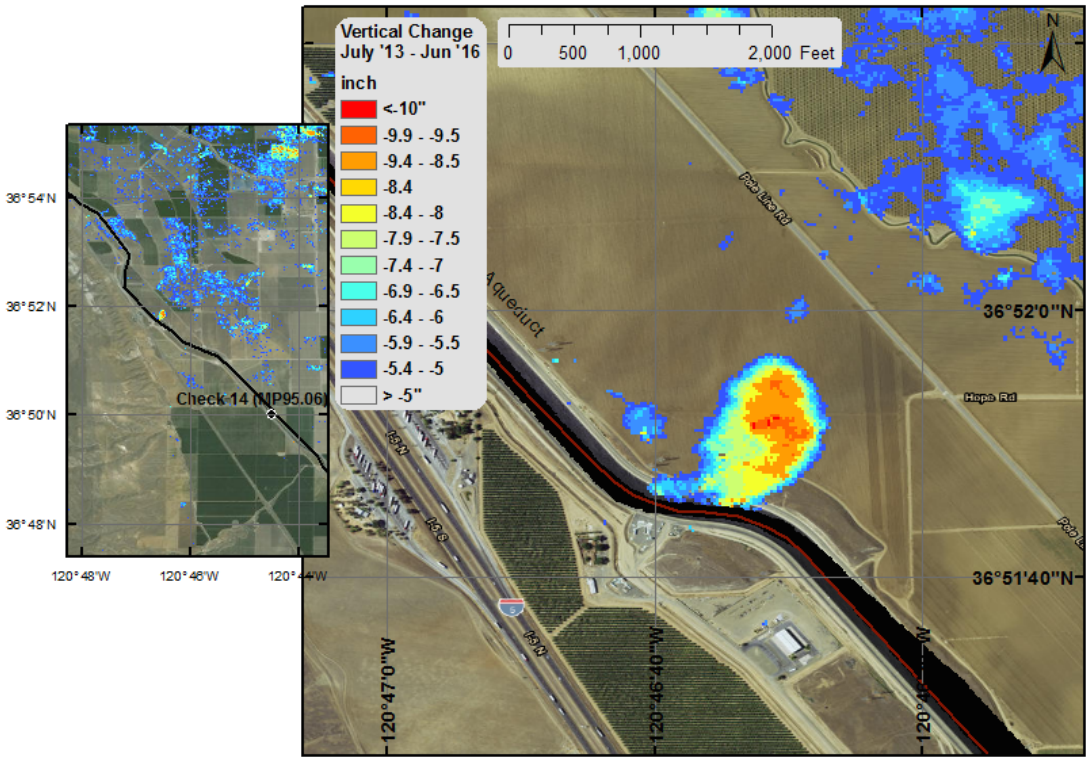

Figure 9. Localized subsidence adjacent to and extending into the California Aqueduct, located north of Check 14 (36°51'50"N, 120°46'30"W) [See inset upper left]. Here the maximum subsidence between July 2013 and June 2016 was ~10" at the feature's center and the maximum subsidence of the aqueduct directly was ~8" on the east side. This feature isn't visible in the Sentinel-1A results.

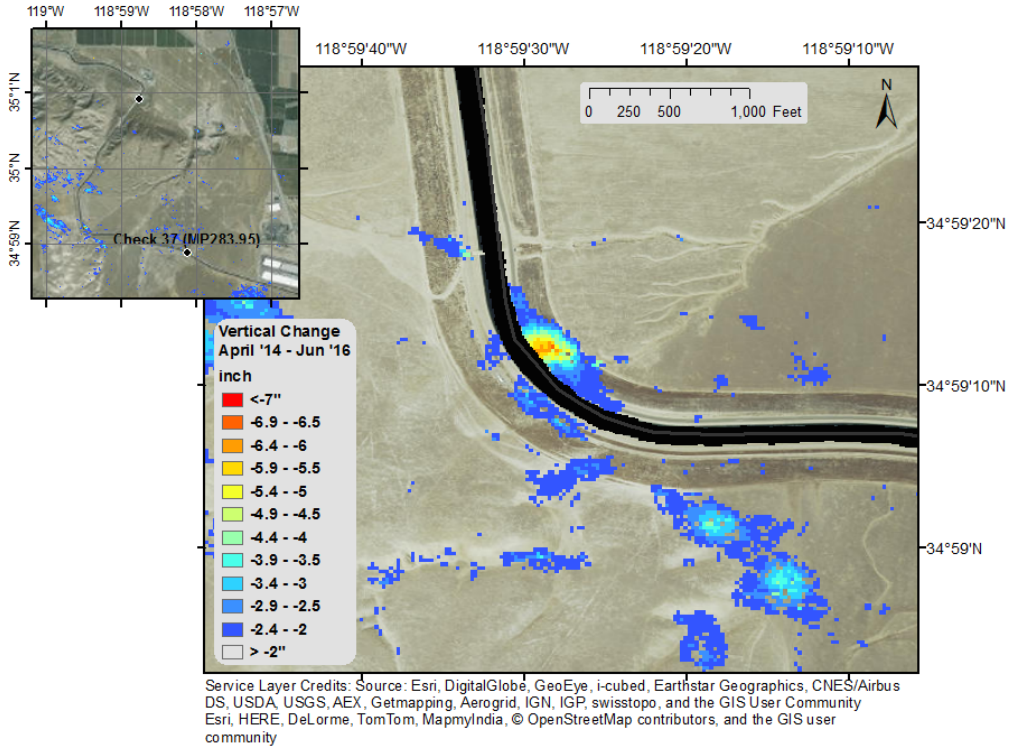

Figure 10. Small subsidence bowl centered on the east side of the aqueduct at 34°59’’12”N, 118°59’30”W. This location is south of the Wind Gap Pumping Plant and north of Check 37 (Inset upper right). Although the magnitude of subsidence (<7”) is small, its proximity to the aqueduct and the indication that there is a high subsidence gradient directly beneath the aqueduct makes it significant.

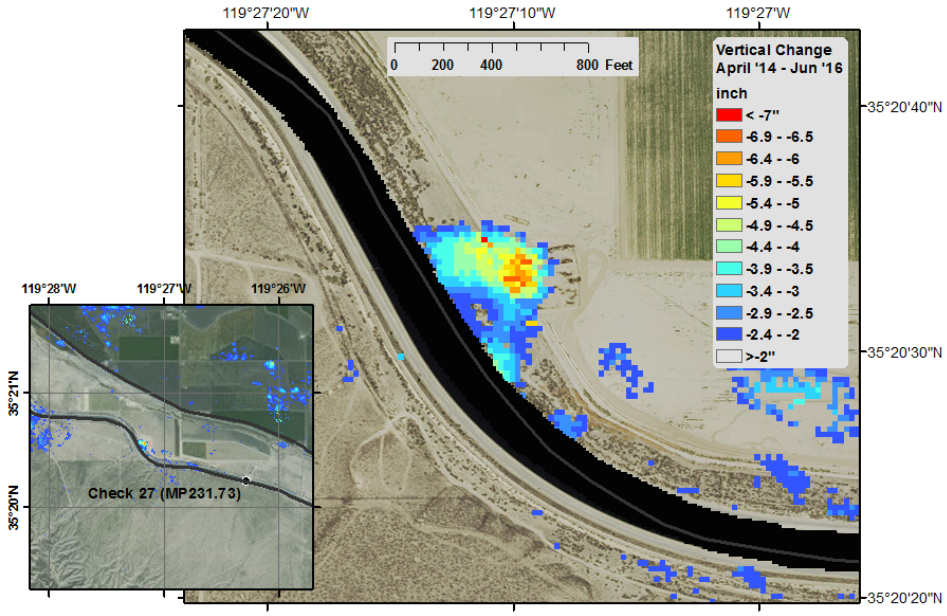

Figure 11. Small subsidence feature in the shape of an arc at 35°20’30”N, 119°27’10”W, north of Check 27, that is centered at the toe of the aqueduct’s east slope. This was identified previously to be the location of a former seep. Maximum impact to the aqueduct is <5” for the period April 2014 to June 2016, however the subsidence continued between Jan. 2015 [Farr et al., 2014] and June 2016, which indicates progress and cumulative subsidence in this localized area.

Subsidence on a broader spatial scale that was measured with UAVSAR continues at all sites reported previously. These are the historically subsiding extended section of the California Aqueduct between Check 16 (MP122.07) and Check 17 (MP132.95) near Cantua Creek (Figure 12); east of Huron, in the vicinity of Check 19 (Figure 13); and near where Old River Rd. crosses the aqueduct, between Check 33 and Check 34 (Figure 14).

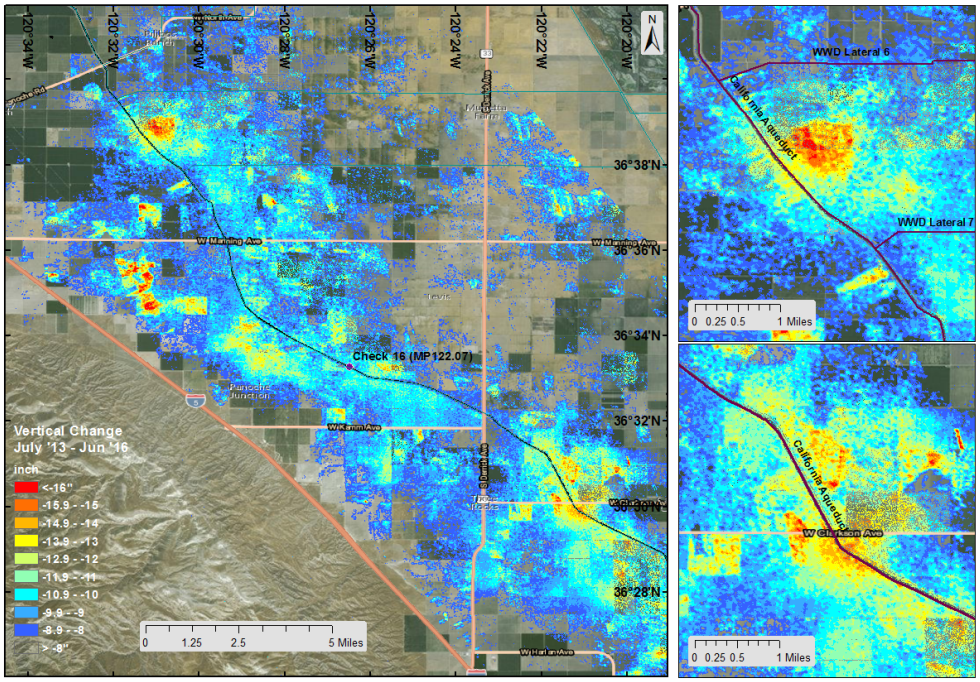

Figure 12. Subsidence near Cantua Creek, affecting an extended section of the California Aqueduct encompassing Checks 16 and 17 that experienced 8" or more of subsidence between July 2013 and June 2016. Two areas showing high subsidence at or near the aqueduct are shown on the right.

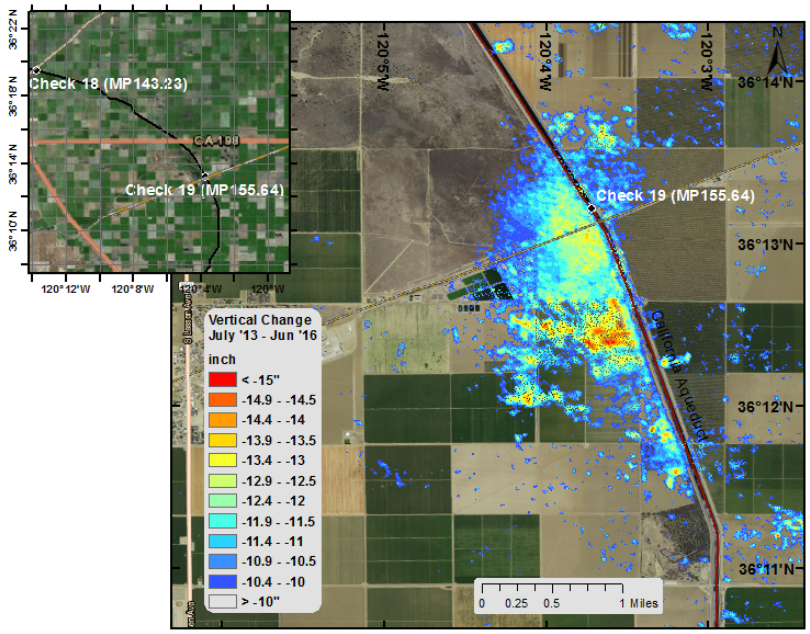

Figure 13. Subsidence in the vicinity of Check 19 east of Huron, which has been persistent since July 2013. An optical image of the wider area is shown at upper left.

One new area identified as having higher subsidence in this longer time series is located in the northern UAVSAR swath (Figure 15). The subsidence appears to extend up to the aqueduct slope but is not yet affecting it greatly. No significant subsidence is identified anywhere along the section of the aqueduct in the environs of the Buena Vista Pumping Plant where a seep developed in 2016 (Figure 16).

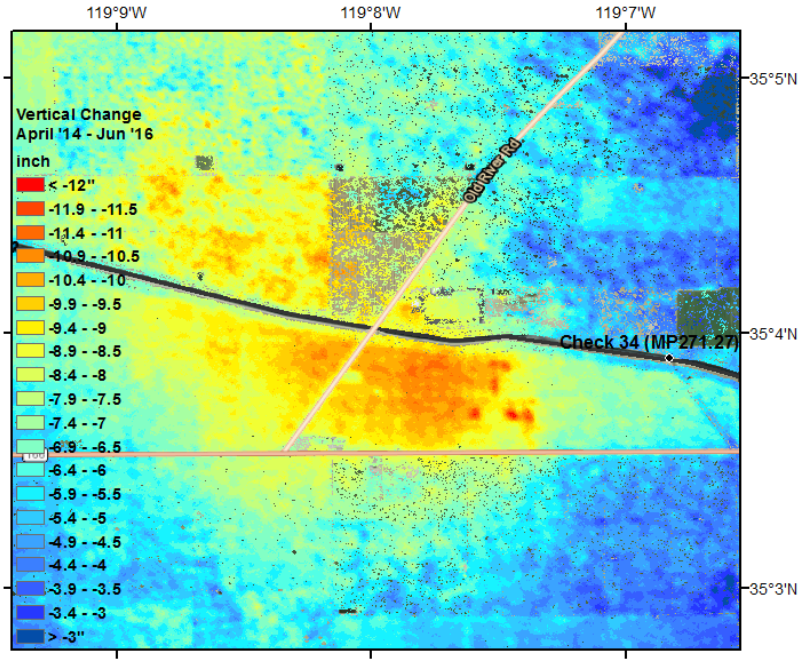

Figure 14. Area of highest widespread subsidence in the southern UAVSAR swath, located just west of Check 34. The highest subsidence of the aqueduct directly is located east of Old River Road.

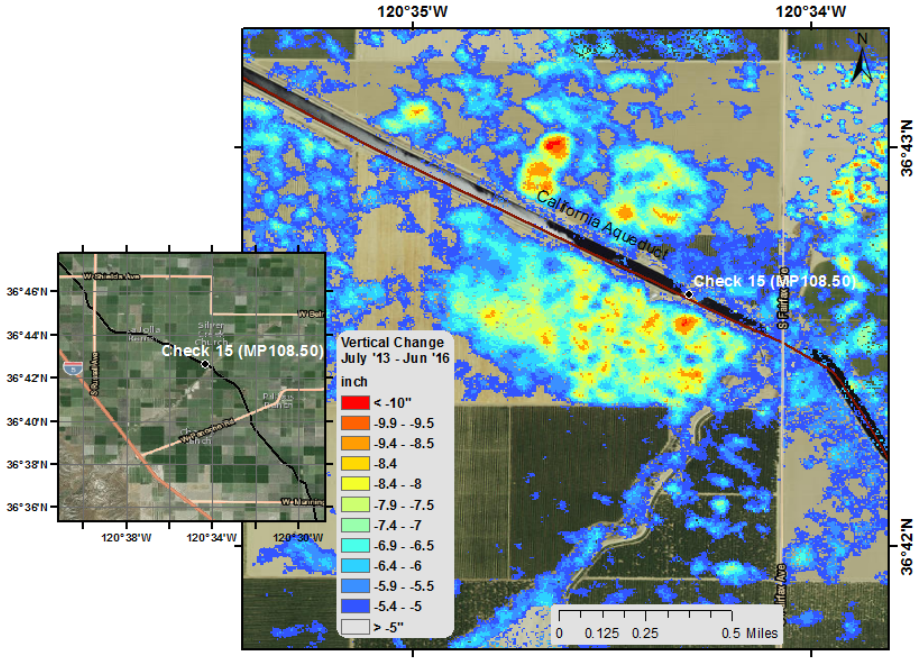

Figure 15. Area near Check 15 where subsidence of 5"-10" has occurred and extends to the toe of the aqueduct along an ~0.5 mile stretch of the west side slope and at two more localized areas on the east side slope.

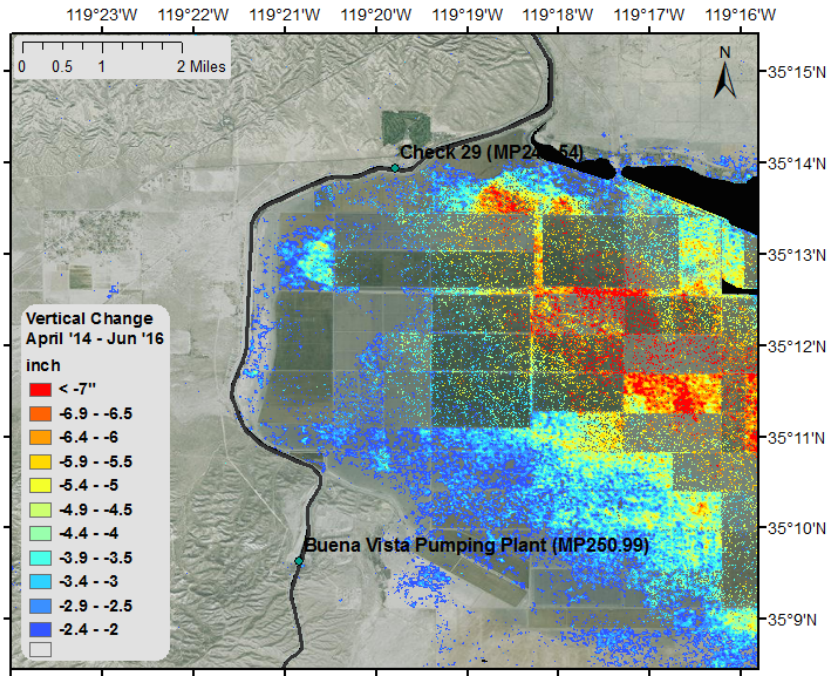

Figure 16. Subsidence map in the general vicinity of Check 29 and the Buena Vista Pumping Plant. Areas in color showed >2" of subsidence during April 2014 and June 2016. No significant subsiding areas in proximity to the aqueduct were identified, however longer term monitoring is needed to identify areas like the one shown in Figure 11.

UAVSAR measured subsidence along part of the Delta-Mendota Canal in addition to the California Aqueduct. Figure 17 shows the one observed area showing high subsidence along this structure.

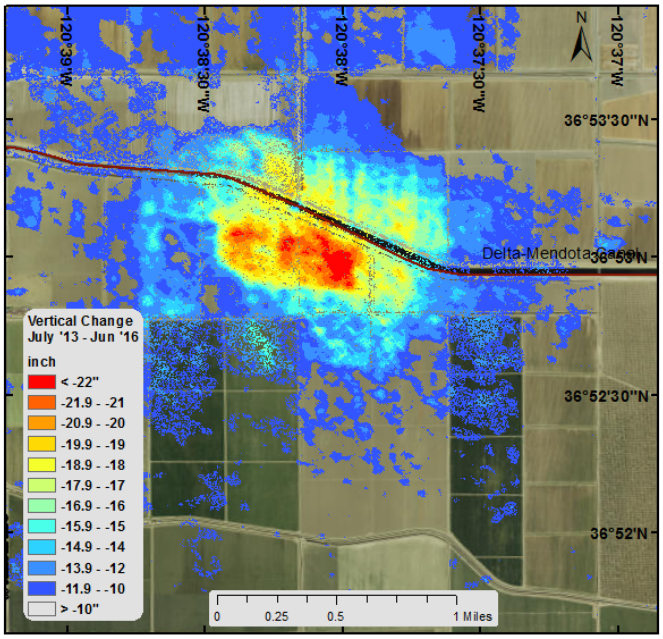

Figure 17. Subsiding section of the Delta-Mendota Canal near 36°53'N, 120°38'W.

Sacramento Valley Subsidence

A subsidence map for the Sacramento Valley using Sentinel-1A data was also produced for this report, covering the period March 1, 2015 to May 30, 2016. This map used data from descending (NE-SW) path #42. The Sacramento Valley subsidence map (Figure 18) shows much less deformation than in the San Joaquin Valley to the south. It also exhibits larger blank areas due to temporal decorrelation caused by small-scale changes in vegetation or plowing.

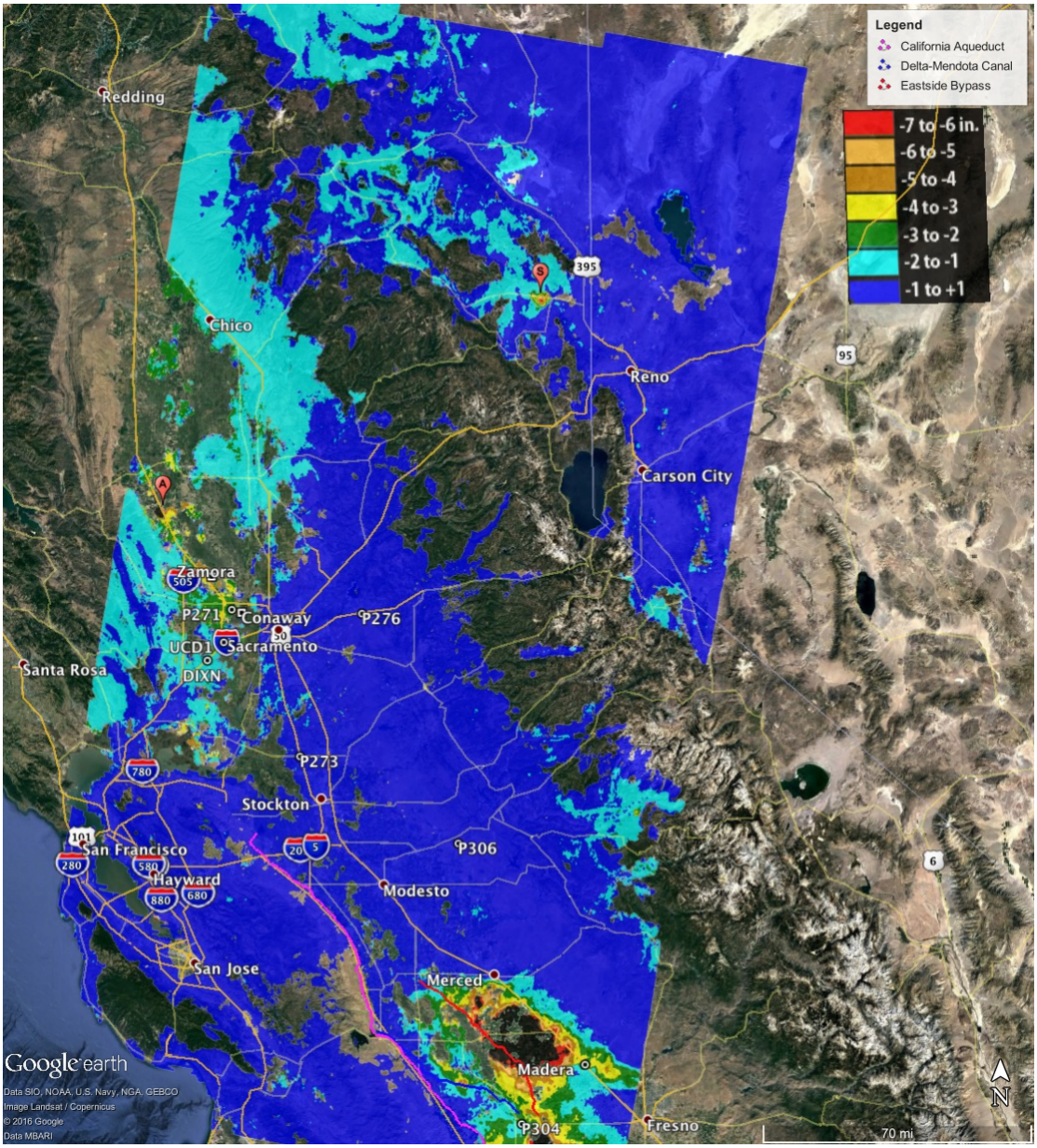

Figure 18. Subsidence map of Sacramento Valley covering the period March 1, 2015 to May 30, 2016 obtained from Sentinel-1A descending pass #42. Note subsidence along the west side of the valley including the Arbuckle area marked 'A' and a small area of subsidence in Sierra Valley, marked 'S', N of Lake Tahoe. The much larger subsidence in the El Nido area shows up at the bottom of the map. Note that the color scale is much different than that for Figure 1 as the subsidence amounts are much less.

Around Woodland and Davis, sites of previous subsidence, subsidence occurs in small areas up to about 2". A small area on the west side of the valley at Arbuckle, noted in the previous report continued to subside until the end of 2015. Total subsidence for the period of observations was about 12" (Fig. 19). A previously un-reported area of subsidence was found in the map in Sierra Valley (~39.8°N, 120.25°W). Recent reports (CA DWR, 2003; http://sierravalleygmd.org/updates.html) indicate increased use of groundwater there along with hydrogeology conducive to compaction and subsidence. A contour map of groundwater level declines (http://sierravalleygmd.org/updates.html) matches the zone of subsidence. Maximum subsidence in the area was about 6"; the history of deformation of the area is shown in Fig. 19.

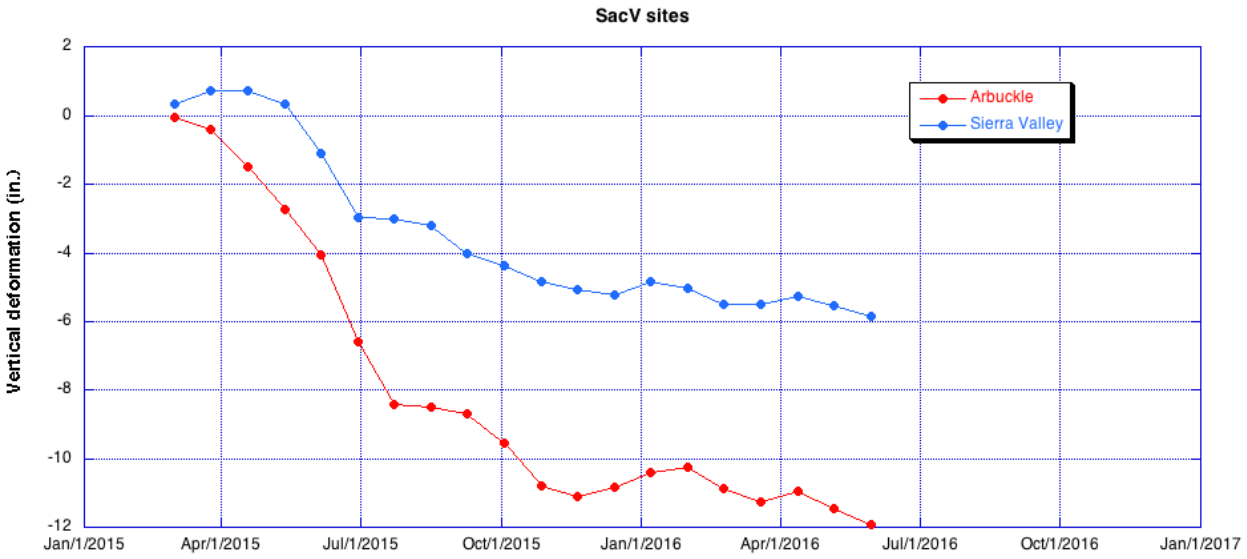

Figure 19. Subsidence histories of two locations in the Sacramento Valley from Sentinel-1A descending pass #42 (Fig. 18). Note the large subsidence in Sierra Valley which corresponds to an area of significant drawdown in the local wells. Arbuckle was identified in the previous report as having exceptionally large subsidence. The trend continued until about Nov. 2015 when subsidence slowed.

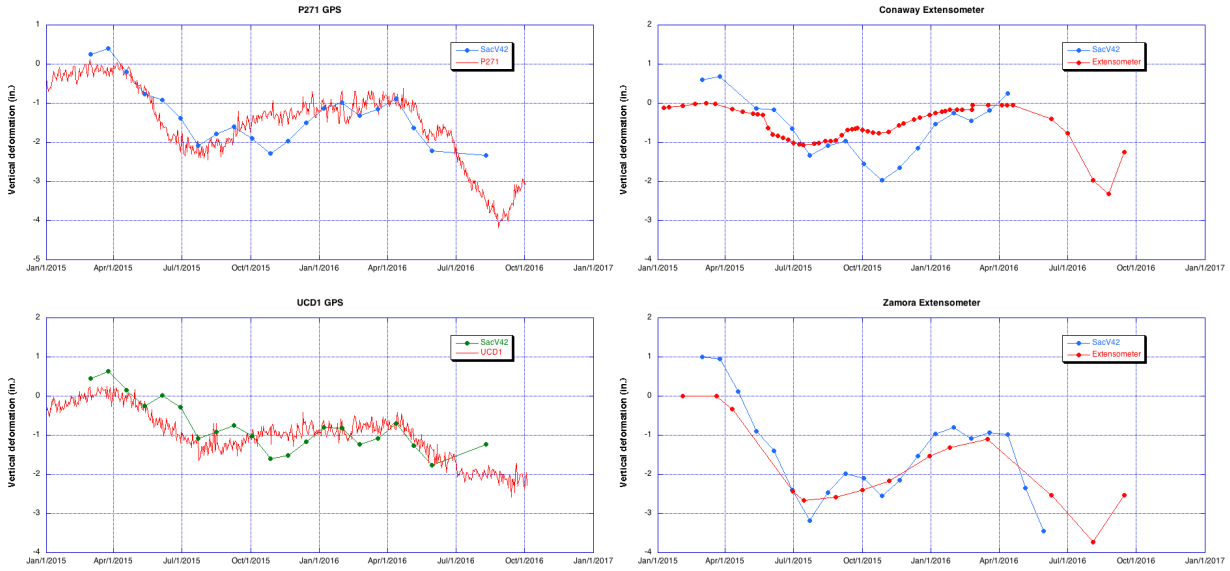

Figure 20. Selected comparisons of GPS vertical time series and InSAR time series at the same locations in the Sacramento Valley projected to vertical. InSAR time series have been arbitrarily offset vertically for an optimal match to the GPS time series. GPS sites are shown in Figure 18. All plots have the same range of Y values (6") and the same date range. Note some deviations, most likely due to water vapor variations affecting the InSAR phase measurements.

Santa Clara Valley Deformation

A deformation map for the Santa Clara Valley was produced by colleagues at Arizona State University, University of California Berkeley, and JPL (Shirzaei et al., 2016) and they have kindly allowed us to reformat it and present as Figure 21. The period covered is March 1, 2015 to March 7, 2016 and, as shown by the map, the overall deformation is uplift which is a maximum of about 1" over the time period. The deformation history of the maximum location is shown in Figure 22 and shows small variations throughout the year, but a general upward trend.

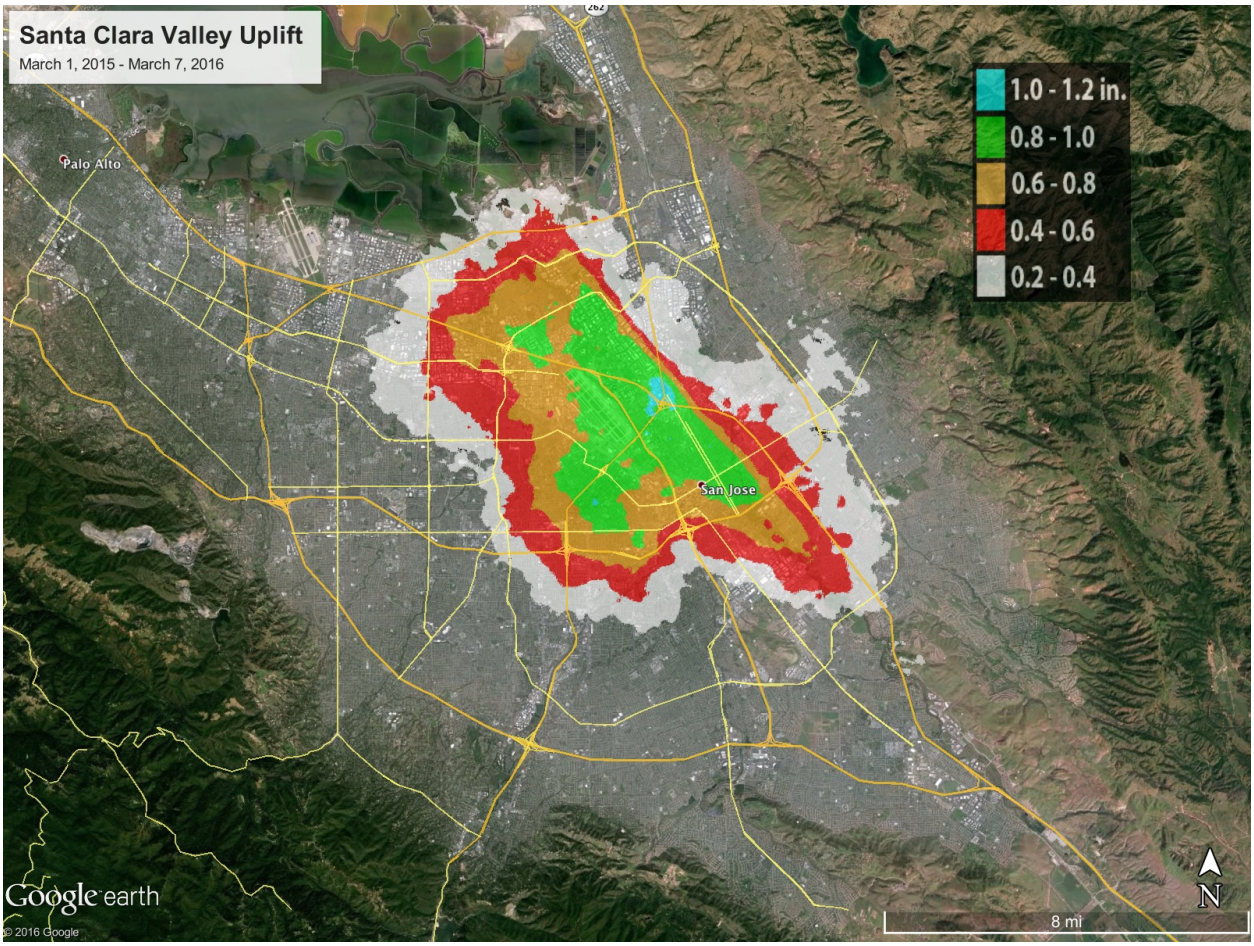

Figure 21. Total subsidence in the Santa Clara Valley for the period March 1, 2015 – March 7, 2016 as measured by ESA's Sentinel-1A, descending path #42 (Shirzaei et al., 2016). The straight edge of the color map is caused by the influence of the Silver Creek Fault.

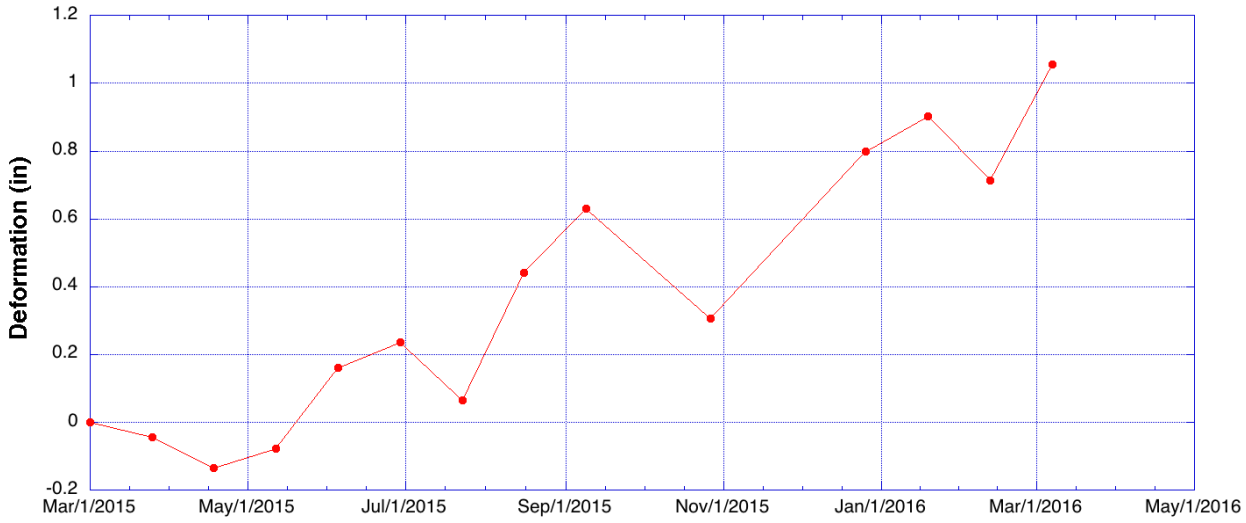

Figure 22. Deformation history of the location of maximum deformation in the Santa Clara Valley. Note that the location is generally uplifting, with short periods of small amounts of subsidence.

South-Central Coast region

The same ascending path #137 used in the San Joaquin Valley also covered the south-central coastal region of California (Fig. 23). The main interest was the coastal flood plain of the Santa Clara River (Oxnard Plain), but the processed area extended west along the coast to Point Conception, east into the Los Angeles basin, and north to the south end of the San Joaquin Valley. For the processed period (May 7, 2015 – August 17, 2016) isolated areas of up to 2" of subsidence were noted in the Oxnard Plain as well as a fairly large zone of up to 2.5" subsidence in the foothills north of Carpinteria. The known subsidence of Cuyama Valley also shows up as well as various isolated areas in other alluvial basins in the area. Pixel histories are shown in Fig. 24 for some of these features.

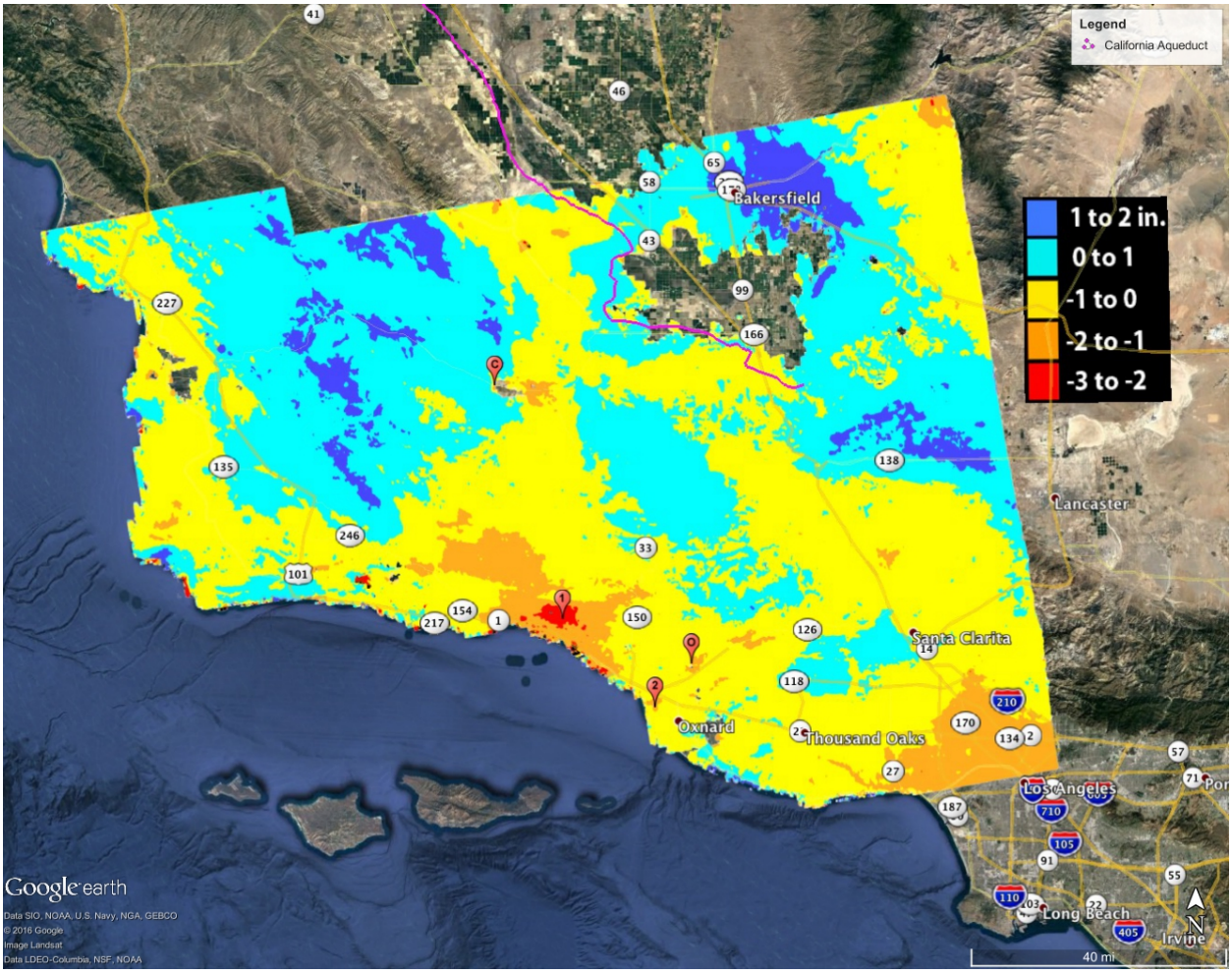

Figure 23. Subsidence in the south-central coast region of California, including Ventura, Santa Barbara and north to the San Joaquin Valley covering the period May 7, 2015 – August 17, 2016. This path (ascending #137) covers the Central Valley as well (Fig. 1). Note a large area in the foothills above Carpinteria (#1) which could be due to atmospheric water vapor, small patches of subsidence in the Oxnard Plain (#2, O), and subsidence in the Cuyama Valley (C).

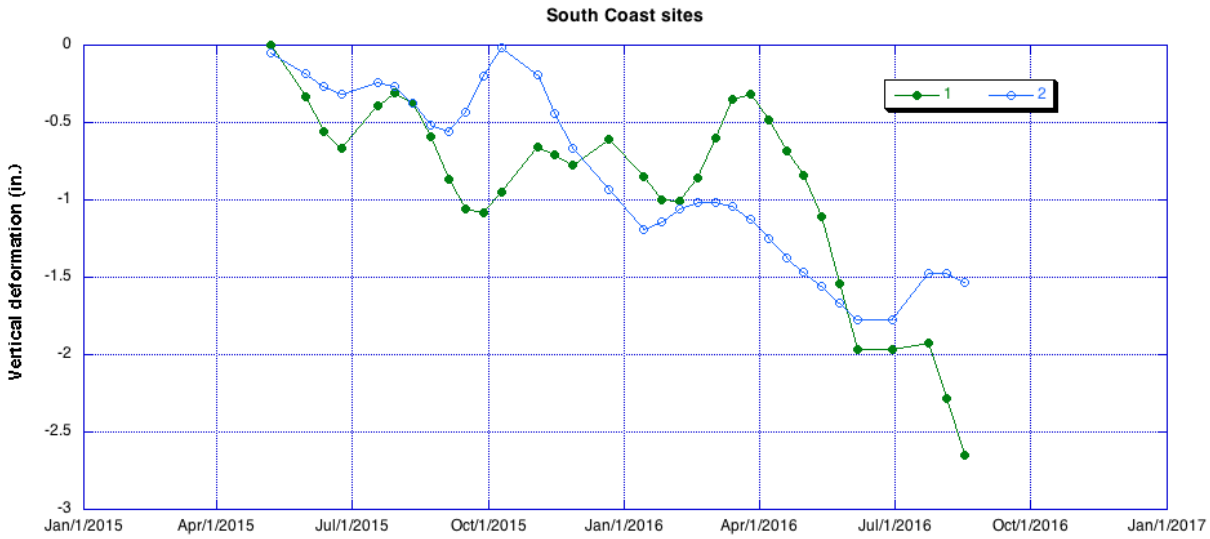

Figure 24. Subsidence histories for 2 locations in the south-central coast region from Sentinel-1A ascending pass #137 (Fig. 23). The numbered curves are indicated on the map: 1= area N of Carpinteria, 2 = site in Oxnard Plain.

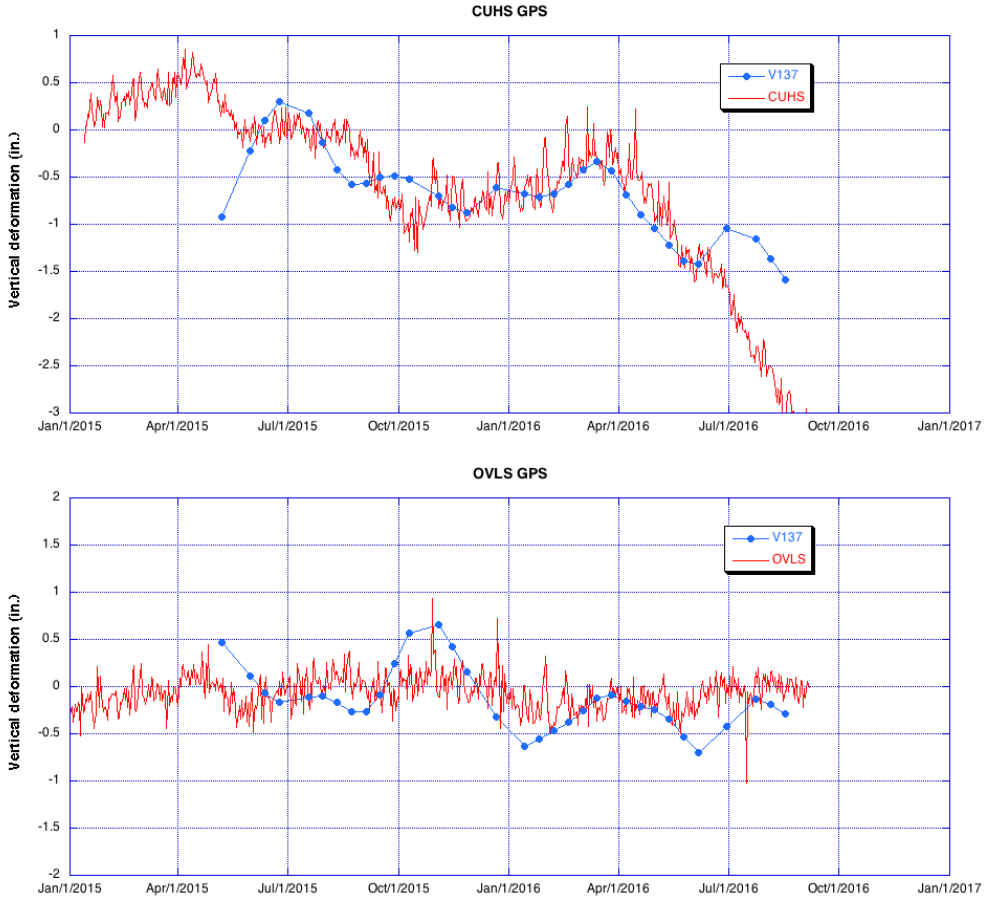

Figure 25. Selected comparisons of GPS vertical time series and InSAR time series at the same locations in the South Coast region projected to vertical. InSAR time series have been arbitrarily offset vertically for an optimal match to the GPS time series. GPS sites are shown in Figure 23 ('C' is CUHS and 'O' is OVLS). Both plots have the same range of Y values (4") and the same date range. Note some deviations, most likely due to water vapor variations affecting the InSAR phase measurements.

Conclusions and Future Plans

Sentinel-1A, launched in April 2014, has proved to be useful for making maps of subsidence in alluvial basins of California. Maps as well as pixel histories of subsidence and transects showing temporal and spatial details of subsidence can be produced from the InSAR data. Updates of the subsidence maps for California will continue with Sentinel-1B, launched in April 2016, joining its twin in orbit. The first acquisitions for California by Sentinel-1A were in late 2014 and are continuing, in general every 12-24 days. Early acquisitions over California were more sporadic, but have become more reliable as the coverage area has expanded along with ESA's capability to collect and process the data. We have begun downloading and processing Sentinel-1 data for other basins of California, including Antelope Valley, Coachella Valley, Borrego Valley, and the Salinas Valley, along with coastal areas. As the database expands, we expect to be able to present maps of those areas, as well as continuing monitoring of the Central Valley. Figure 26 shows the coverage of Sentinel-1A over California used for this report.

The high spatial resolution and low instrument noise of the UAVSAR is shown to accurately measure subsidence along the California Aqueduct and elsewhere in its swath both over large areas and, of particular value, on a much more localized scale. The UAVSAR results reported here focus on showing the small-scale subsidence directly impacting the aqueduct and identify two new such features in addition to one new area of broader areal subsidence. Furthermore, subsidence is shown not to be rapid in the vicinity of the repaired section near the Buena Vista Pumping Plant. Acquisition of the UAVSAR lines will continue in 2016-2017 and could in principle be expanded to cover more of the Central Valley.

As described above, the InSAR time series we produce are essentially series of maps representing the change in surface elevation for each satellite or airborne radar acquisition date. In a sense, we produce 4-dimensional data sets. For the satellite results we have found that a convenient format for storage and post-processing is a multi-band GeoTiff format, where each 'band' is an acquisition date. Most common Geographic Information System software packages recognize this format and can display map products from the data. We furnish all of the satellite products to the DWR in this format for future use and generation of additional products, although the newer HDF5 format could be a future choice.

The UAVSAR data files for each time step are so large that the files are delivered as GIS rasters with header files for each time step. The cumulative vertical displacement for the entire time series is in the data of the last time step. UAVSAR results are also available as a single HDF5 file for each image swath upon request.

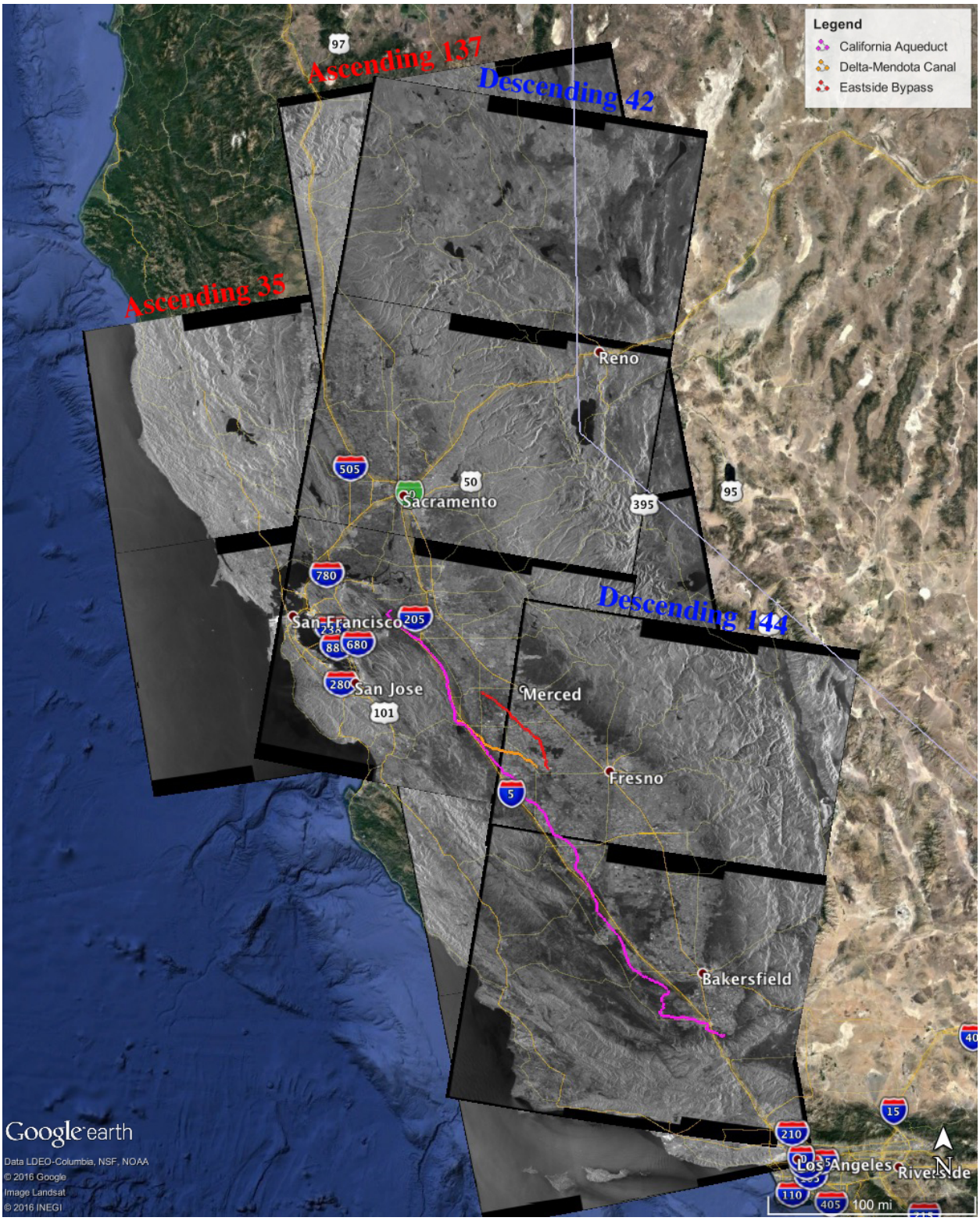

Figure 26. Coverage of Sentinel-1A over California used for this report. Ascending (SE-NW) path 137 passes from Ventura through the San Joaquin and Sacramento Valleys and descending (NE-SW) path 42 covers the Santa Clara and Sacramento Valleys. Other paths have been acquired and processed for cross-calibration and verification purposes.

Acknowledgements

This work was funded by the California Department of Water Resources. This work was carried out at the Jet Propulsion Laboratory, California Institute of Technology, under contract with NASA. UAVSAR data are courtesy NASA/JPL-Caltech. The Alaska Satellite Facility (http://www.asf.alaska.edu/) archives and distributes the Sentinel-1A and UAVSAR data used in this report. Copyright 2016 California Institute of Technology. U.S. Government sponsorship acknowledged.

References

Amelung, F., D.L. Galloway, J.W. Bell, H.A. Zebker, R.J. Laczniak, 1999, Sensing the ups and downs of Las Vegas: InSAR reveals structural control of land subsidence and aquifer-system deformation, Geology, v. 27, p. 483-486.

Bawden, G.W., W. Thatcher, R.S. Stein, K.W. Hudnut, G. Peltzer, 2001, Tectonic contraction across Los Angeles after removal of groundwater pumping effects, Nature, v. 412, p. 812-813.

Bekaert, D. P. S., R. J. Walters, T. J. Wright, A Hooper, and D. J Parker (2015), Statistical comparison of InSAR tropospheric correction techniques, *Remote Sensing of Environment*, v. 170, p. 40-47, doi:10.1016/j.rse.2015.08.035.

Bell, J.W., F. Amelung, A. Ferretti, M. Bianchi, F. Novali, 2008, Permanent scatterer InSAR reveals seasonal an long-term aquifer-system response to groundwater pumping and artificial recharge, Water Resources Research, v. 44, doi: 10.1029/2007WR006152.

Berardino, P., G. Fornaro, R. Lanari, E. Sansosti, 2002, A new algorithm for surface deformation monitoring based on small baseline differential SAR interferograms, IEEE Trans. Geosci. Remote Sensing, v. 40, doi:10.1109/TGRS.2002.803792.

Bertoldi, G.L., R.H. Johnston, K.D. Evenson, 1991, Ground water in the Central Valley, California—A summary report, U.S. Geological Survey Professional Paper 1401-A, 44 p.

Borchers, J.W., M. Carpenter, 2014, Land Subsidence from Groundwater Use in California, Report of Findings to the California Water Foundation, http://www.californiawaterfoundation.org

CA DWR, 2003, California's Groundwater, DWR Bulletin 118, update 2003.

Calderhead, A.I., R. Therrien, A. Rivera, R. Martel, J. Garfias, 2011, Simulating pumping-induced regional land subsidence with the use InSAR and field data in the Toluca Valley, Mexico, Adv. Water Resources, v. 34, p. 83-97, doi:10.1016/j.advwatres.2010.09.017.

Chaussard, E., F. Amelung, H. Abidin, S-H. Hong, 2013, Sinking cities in Indonesia: ALOS PALSAR detects rapid subsidence due to groundwater and gas extraction, Rem. Sens. Env., v. 128, p. 150-161.

Deverel, S.J., D.A. Leighton, 2010, Historic, recent, and future subsidence, Sacramento-San Joaquin Delta, California, USA, San Francisco Estuary and Watershed Science, v. 8.

Donnellan, A., J. Parker, S. Hensley, M. Pierce, J. Wang, J. Rundle, 2014, UAVSAR observations of triggered slip on the Imperial, Superstition Hills, and East Elmore Ranch Faults associated with the 2010 M 7.2 El Mayor – Cucapah earthquake, Geochemistry, Geophysics, Geosystems, v. 15, p. 815-829.

Farr, T.G., 2011, Remote monitoring of groundwater with orbital radar, abs., Groundwater Resources Assoc. Ann. Mtg., Sacramento, CA. http://www.grac.org/am2011.asp

Farr, T.G., Z. Liu, 2015, Monitoring Subsidence Associated with Groundwater Dynamics in the Central Valley of California Using Interferometric Radar, Ch. 24 in Remote Sensing of the Terrestrial Water Cycle, Geophysical Monograph 206, V. Lakshmi, ed., American Geophysical Union, John Wiley & Sons, Inc.

Farr, T.G., C. Jones, Z. Liu, 2015, Progress report: Subsidence in the Central Valley, California, submitted to CA DWR. Available at: http://www.nasa.gov/jpl/nasa-california-drought-causing-valley-land-to-sink.

Galloway, D.L., D.R. Jones, S.E. Ingebritsen, 1999, Land subsidence in the United States. U.S. Geological Survey Circular 1182, 175 p.

Galloway, D.L., K.W. Hudnut, S.E. Ingebritsen, S.P. Phillips, G. Peltzer, F. Rogez, P.A. Rosen, 1998, Detection of aquifer system compaction and land subsidence using interferometric synthetic aperture radar, Antelope Valley, Mojave Desert, California, Water Resources Research, v. 34, p. 2573-2585.

Hoffmann, J., H.A. Zebker, D.L. Galloway, F. Amelung, 2001, Seasonal subsidence and rebound in Las Vegas Valley, Nevada, observed by synthetic aperture radar interferometry, Water Resources Research, v. 37, p. 1551-1566.

Jones, C. E., G. Bawden, S. Deverel, J. Dudas, S. Hensley, S.-H. Yun, 2012, Study of movement and seepage along levees using DINSAR and the airborne UAVSAR instrument, In *Proc. SPIE* 8536, *SAR Image Analysis, Modeling, and Techniques XII*, 85360E, International Society for Optics and Photonics, doi:10.1117/12.976885.

Jones, C. E., R. G. Blom, 2014, Bayou Corne, Louisiana, sinkhole: Precursory deformation measured by radar interferometry, Geology, v. 42, p. 111-114.

Jones, C. E., J. Dudas, G. W. Bawden, 2016, Application of remote sensing to assessment of water conveyance infrastructure integrity. In R. L. Anderson and H. Ferriz (Eds.), *Applied*

Geology in California, Special Publication 26, Association of Environmental and Engineering Geologists, Star Publishing Company.

Lanari, R., P. Lundgren, M. Manzo, F. Casu, 2004, Satellite radar interferometry time series analysis of surface deformation for Los Angeles, California, Geophys. Res. Lett., v. 31, doi: 10.1029/2004GL021294.

Lu, Z., W.R. Danskin, 2001, InSAR analysis of natural recharge to define structure of a ground-water basin, San Bernardino, California, Geophys. Res. Lett., v. 28, p. 2661-2664.

Lundgren, P., F. Casu, M. Manzo, A. Pepe, P. Berardino, E. Sansosti, R. Lanari, 2004, Gravity and magma induced spreading of Mount Etna volcano revealed by satellite radar interferometry, Geophys. Res. Lett., v. 31, L04602.

Lundgren, P., E. A. Hetland, Z. Liu, and E. J. Fielding, 2009, Southern San Andreas-San Jacinto fault system slip rates estimated from earthquake cycle models constrained by GPS and interferometric synthetic aperture radar observations, J. Geophys. Res., v. 114, B02403, doi:10.1029/2008JB005996.

Madsen, S.N., H.A. Zebker, 1998, Imaging Radar Interferometry, ch. 6, p. 359-380, in Henderson, F.M., A.J. Lewis, ed., 1998, Principles and Applications of Imaging Radar, Manual of Remote Sensing, v. 2, Wiley, NY, 866 pp.

Massonnet, D., 1997, Satellite radar interferometry, Scientific American, v. 276, Feb., p. 46-53.

Ozawa, T., H. Ueda, 2011, Advanced interferometric synthetic aperture radar (InSAR) time series analysis suing interferograms of multiple-orbit tracks: a case study on Miyake-Jima, J. Geophys. Res., 116, B12407, doi:10.1029/2011JB008489.

Reeves, J.A., R.J. Knight, H. Zebker, W.A. Schreüder, P.S. Agram, and T.R. Lauknes, 2011, High quality InSAR data linked to seasonal change in hydraulic head for an agricultural area in the San Luis Valley, Colorado, WRR, v. 47, DOI: 10.1029/2010WR010312.

Sansosti, E., F. Casu, M. Manzo, R. Lanari, 2010, Space‐borne radar interferometry techniques for the generation of deformation time series: An advanced tool for Earth's surface displacement analysis, Geophys. Res. Lett., v. 37, L20305, doi:10.1029/2010GL044379.

Sharma, P., C. E. Jones, J. Dudas, G. Bawden, S. Deverel, 2016, Monitoring of subsidence with UAVSAR on Sherman Island in California's Sacramento-San Joaquin delta. *Remote Sensing of Environment*, *181*, 218-236, doi:10.1016/j.rse.2016.04.012.

Shirzaei, M., R. Bürgmann and E. Fielding, 2016, Sentinel-1 TOPS multitemporal interferometry for monitoring slow ground motions in the San Francisco Bay Area, Geophysical Research Letters, submitted.

Sneed, M., and Brandt, J.T., 2013, Detection and measurement of land subsidence using global positioning system surveying and Interferometric Synthetic Aperture Radar, Coachella Valley, California, 1996-2005: U.S. Geological Survey Scientific Investigations Report 2007-5251, v. 2.0, 31 p.

Sneed, M., S.V. Stork, R.J. Laczniak, 2003, Aquifer-system characterization using InSAR, in K.R. Prince and D.L. Galloway, eds., US Geological Survey subsidence interest group conference proceedings, 2001, USGS Open-File Rept. 03-308.

Sneed, M., and Brandt, J.T., 2007, Detection and measurement of land subsidence using global positioning system surveying and Interferometric Synthetic Aperture Radar, Coachella Valley, California, 1996-2005: U.S. Geological Survey Scientific Investigations Report 2007-5251, 31 p.

Appendix: Detailed lists of data used

Sentinel-1A Data Listing

Data from the Sentinel-1A satellite of the European Space Agency (ESA) was used for this report. Data were obtained from the Alaska Satellite Facility (https://www.asf.alaska.edu). See Table 1 for some characteristics of the instrument. All data for the San Joaquin Valley was from a single orbital path, repeated approximately every 24 days. The path was ascending (SE to NW) number 137, shown in Figure 26. The same path was also extended into the Sacramento Valley, though fewer dates were acquired. A descending path, number 42 was also processed for the Sacramento Valley. That path had acquisitions every 24 days and for a longer time period, allowing more reliable results. The San Joaquin and Sacramento Valleys were processed separately to keep data volumes manageable and because the maximum amount of deformation was very different in the two areas.

Sentinel-1A acquires data in a modified scan-SAR mode called Interferometric Wide Swath mode (IW). Swaths are broken into 3 subswaths across-track and into frames along track, which are stitched together in the processing. VV polarization was used for all InSAR products and the incidence angle varies from 29° to 46°. Details of the frames used are given below.

Table A1. Details of Sentinel-1A frames used for this report.

San Joaquin Valley (ascending path 137)

Granule Name	Absolute Orbit	Path Number	Frame Number	Acquisition Date	Center Lat	Center Lon
S1A_IW_SLC__1SSV_20150507T015909_20150507T015936_005809_007783_0A02	5809	137	121	2015-05-07T01:59:36Z	38.2032	-120.6027
S1A_IW_SLC__1SSV_20150507T015934_20150507T020001_005809_007783_21B0	5809	137	126	2015-05-07T02:00:01Z	39.7114	-120.9421
S1A_IW_SLC__1SSV_20150507T015958_20150507T020025_005809_007783_DEA7	5809	137	131	2015-05-07T02:00:25Z	41.4371	-121.1492
S1A_IW_SLC__1SSV_20150531T015902_20150531T015926_006159_008023_120E	6159	137	120	2015-05-31T01:59:26Z	37.491	-120.4462
S1A_IW_SLC__1SSV_20150531T020001_20150531T020028_006159_008023_74F2	6159	137	132	2015-05-31T02:00:28Z	41.2588	-121.298
S1A_IW_SLC__1SDV_20150612T015903_20150612T015929_006334_008542_88F9	6334	137	120	2015-06-12T01:59:29Z	37.5956	-120.469
S1A_IW_SLC__1SSV_20150624T015904_20150624T015931_006509_008A40_A0B8	6509	137	120	2015-06-24T01:59:31Z	37.7136	-120.4952
S1A_IW_SLC__1SSV_20150624T015928_20150624T015955_006509_008A40_C87F	6509	137	125	2015-06-24T01:59:55Z	39.4463	-120.7098
S1A_IW_SLC__1SSV_20150624T015953_20150624T020020_006509_008A40_2C1B	6509	137	130	2015-06-24T02:00:20Z	40.7298	-121.1763
S1A_IW_SLC__1SSV_20150718T015904_20150718T015931_006859_0093FC_2DF5	6859	137	119	2015-07-18T01:59:31Z	37.7148	-120.4898
S1A_IW_SLC__1SSV_20150718T015929_20150718T015956_006859_0093FC_A1F8	6859	137	125	2015-07-18T01:59:56Z	39.2232	-120.8273
S1A_IW_SLC__1SSV_20150718T015954_20150718T020021_006859_0093FC_8A55	6859	137	129	2015-07-18T02:00:21Z	40.731	-121.1709
S1A_IW_SLC__1SDV_20150730T015905_20150730T015931_007034_0098F3_B456	7034	137	120	2015-07-30T01:59:31Z	37.9261	-120.3837
S1A_IW_SLC__1SSV_20150811T015905_20150811T015932_007209_009DB6_0927	7209	137	120	2015-08-11T01:59:32Z	37.7152	-120.4907
S1A_IW_SLC__1SSV_20150811T015930_20150811T015957_007209_009DB6_9419	7209	137	125	2015-08-11T01:59:57Z	39.2236	-120.8282
S1A_IW_SLC__1SSV_20150811T015955_20150811T020022_007209_009DB6_99FF	7209	137	130	2015-08-11T02:00:22Z	40.7314	-121.1719
S1A_IW_SLC__1SDV_20150823T015906_20150823T015932_007384_00A274_AFD4	7384	137	121	2015-08-23T01:59:32Z	37.5958	-120.4655
S1A_IW_SLC__1SSV_20150904T015906_20150904T015933_007559_00A743_526B	7559	137	120	2015-09-04T01:59:33Z	37.7148	-120.4911
S1A_IW_SLC__1SSV_20150904T015931_20150904T015958_007559_00A743_1B7C	7559	137	125	2015-09-04T01:59:58Z	39.2232	-120.8286
S1A_IW_SLC__1SSV_20150904T015956_20150904T020023_007559_00A743_AC5B	7559	137	130	2015-09-04T02:00:23Z	40.731	-121.1722
S1A_IW_SLC__1SSV_20150928T015907_20150928T015928_007909_00B0A5_9B50	7909	137	121	2015-09-28T01:59:28Z	37.4295	-120.4276
S1A_IW_SLC__1SDV_20151010T015907_20151010T015934_008084_00B54A_36FA	8084	137	120	2015-10-10T01:59:34Z	37.5958	-120.4645
S1A_IW_SLC__1SDV_20151103T015907_20151103T015933_008434_00BEB3_6450	8434	137	121	2015-11-03T01:59:33Z	37.5959	-120.4655
S1A_IW_SLC__1SSV_20151115T015902_20151115T015928_008609_00C380_10D6	8609	137	120	2015-11-15T01:59:28Z	37.382	-120.4172
S1A_IW_SLC__1SSV_20151115T015926_20151115T015953_008609_00C380_A7AA	8609	137	125	2015-11-15T01:59:53Z	38.8905	-120.7534
S1A_IW_SLC__1SSV_20151115T015951_20151115T020018_008609_00C380_C5FA	8609	137	130	2015-11-15T02:00:18Z	40.3984	-121.0957
S1A_IW_SLC__1SDV_20151127T015901_20151127T015927_008784_00C867_764C	8784	137	119	2015-11-27T01:59:27Z	37.2628	-120.3904
S1A_IW_SLC__1SDV_20151221T015900_20151221T015926_009134_00D232_39D0	9134	137	119	2015-12-21T01:59:26Z	37.2626	-120.3912
S1A_IW_SLC__1SDV_20160114T015859_20160114T015925_009484_00DC2E_A309	9484	137	119	2016-01-14T01:59:25Z	37.2627	-120.3912
S1A_IW_SLC__1SSV_20160126T015924_20160126T015951_009659_00E14D_F626	9659	137	124	2016-01-26T01:59:51Z	38.8903	-120.7528

S1A_IW_SLC__1SDV_20160207T015809_20160207T015836_009834_00E65A_9D60	9834	137	109	2016-02-07T01:58:36Z	34.3632	-119.76
S1A_IW_SLC__1SDV_20160207T015834_20160207T015901_009834_00E65A_8B5F	9834	137	114	2016-02-07T01:59:01Z	35.8727	-120.0862
S1A_IW_SLC__1SDV_20160207T015859_20160207T015925_009834_00E65A_2B96	9834	137	119	2016-02-07T01:59:25Z	37.2627	-120.3912
S1A_IW_SLC__1SSV_20160219T015809_20160219T015836_010009_00EB80_E840	10009	137	109	2016-02-19T01:58:36Z	34.3633	-119.7605
S1A_IW_SLC__1SSV_20160219T015834_20160219T015901_010009_00EB80_7948	10009	137	113	2016-02-19T01:59:01Z	35.8727	-120.0868
S1A_IW_SLC__1SSV_20160219T015859_20160219T015926_010009_00EB80_9A87	10009	137	119	2016-02-19T01:59:26Z	37.3818	-120.4177
S1A_IW_SLC__1SDV_20160302T015809_20160302T015836_010184_00F077_C0AC	10184	137	108	2016-03-02T01:58:36Z	34.3632	-119.7616
S1A_IW_SLC__1SDV_20160302T015834_20160302T015901_010184_00F077_5DCF	10184	137	113	2016-03-02T01:59:01Z	35.8727	-120.0879
S1A_IW_SLC__1SDV_20160302T015859_20160302T015925_010184_00F077_2231	10184	137	119	2016-03-02T01:59:25Z	37.2626	-120.3929
S1A_IW_SLC__1SDV_20160314T015817_20160314T015845_010359_00F590_5287	10359	137	110	2016-03-14T01:58:45Z	34.8522	-119.8666
S1A_IW_SLC__1SDV_20160314T015842_20160314T015909_010359_00F590_F69F	10359	137	116	2016-03-14T01:59:09Z	36.3615	-120.1943
S1A_IW_SLC__1SDV_20160314T015907_20160314T015934_010359_00F590_7536	10359	137	121	2016-03-14T01:59:34Z	37.8704	-120.5269
S1A_IW_SLC__1SDV_20160326T015810_20160326T015837_010534_00FA6A_4120	10534	137	109	2016-03-26T01:58:37Z	34.3631	-119.7613
S1A_IW_SLC__1SDV_20160326T015835_20160326T015902_010534_00FA6A_6204	10534	137	114	2016-03-26T01:59:02Z	35.8727	-120.0876
S1A_IW_SLC__1SDV_20160326T015859_20160326T015926_010534_00FA6A_8428	10534	137	119	2016-03-26T01:59:26Z	37.2626	-120.3926
S1A_IW_SLC__1SSV_20160407T015810_20160407T015837_010709_00FF8A_150F	10709	137	109	2016-04-07T01:58:37Z	34.3632	-119.7614
S1A_IW_SLC__1SSV_20160407T015835_20160407T015902_010709_00FF8A_8AB5	10709	137	114	2016-04-07T01:59:02Z	35.8727	-120.0877
S1A_IW_SLC__1SSV_20160407T015900_20160407T015927_010709_00FF8A_4AAD	10709	137	119	2016-04-07T01:59:27Z	37.3818	-120.4186
S1A_IW_SLC__1SDV_20160419T015811_20160419T015838_010884_0104D5_C208	10884	137	109	2016-04-19T01:58:38Z	34.3635	-119.7613
S1A_IW_SLC__1SDV_20160419T015835_20160419T015902_010884_0104D5_E20A	10884	137	114	2016-04-19T01:59:02Z	35.873	-120.0876
S1A_IW_SLC__1SDV_20160419T015900_20160419T015926_010884_0104D5_4427	10884	137	119	2016-04-19T01:59:26Z	37.263	-120.3926
S1A_IW_SLC__1SSV_20160501T015811_20160501T015838_011059_010A54_2DAA	11059	137	110	2016-05-01T01:58:38Z	34.3632	-119.7616
S1A_IW_SLC__1SSV_20160501T015836_20160501T015903_011059_010A54_763F	11059	137	115	2016-05-01T01:59:03Z	35.8727	-120.0879
S1A_IW_SLC__1SSV_20160501T015901_20160501T015928_011059_010A54_6D62	11059	137	120	2016-05-01T01:59:28Z	37.3817	-120.4189
S1A_IW_SLC__1SSV_20160501T015926_20160501T015953_011059_010A54_399D	11059	137	124	2016-05-01T01:59:53Z	38.8902	-120.7551
S1A_IW_SLC__1SDV_20160513T015815_20160513T015842_011234_010FDE_B126	11234	137	110	2016-05-13T01:58:42Z	34.5297	-119.7981
S1A_IW_SLC__1SDV_20160513T015840_20160513T015906_011234_010FDE_2455	11234	137	115	2016-05-13T01:59:06Z	36.0392	-120.1249
S1A_IW_SLC__1SDV_20160513T015904_20160513T015942_011234_010FDE_EA32	11234	137	120	2016-05-13T01:59:42Z	37.7621	-120.503
S1A_IW_SLC__1SSV_20160525T015815_20160525T015842_011409_01159A_A7C0	11409	137	110	2016-05-25T01:58:42Z	34.5298	-119.7968
S1A_IW_SLC__1SSV_20160525T015840_20160525T015907_011409_01159A_D99C	11409	137	115	2016-05-25T01:59:07Z	36.0392	-120.1235
S1A_IW_SLC__1SSV_20160525T015905_20160525T015932_011409_01159A_5305	11409	137	120	2016-05-25T01:59:32Z	37.5482	-120.455
S1A_IW_SLC__1SDV_20160606T015816_20160606T015843_011584_011B33_10B8	11584	137	111	2016-06-06T01:58:43Z	34.7982	-119.69
S1A_IW_SLC__1SDV_20160606T015841_20160606T015908_011584_011B33_FA90	11584	137	116	2016-06-06T01:59:08Z	36.0392	-120.1237
S1A_IW_SLC__1SDV_20160606T015906_20160606T015932_011584_011B33_12AE	11584	137	121	2016-06-06T01:59:32Z	37.7606	-120.3443
S1A_IW_SLC__1SDV_20160630T015817_20160630T015844_011934_012632_783B	11934	137	111	2016-06-30T01:58:44Z	34.5299	-119.7979
S1A_IW_SLC__1SDV_20160630T015842_20160630T015909_011934_012632_C2B9	11934	137	116	2016-06-30T01:59:09Z	36.0393	-120.1247
S1A_IW_SLC__1SDV_20160630T015907_20160630T015933_011934_012632_4037	11934	137	121	2016-06-30T01:59:33Z	37.4293	-120.4303
S1A_IW_SLC__1SDV_20160724T015819_20160724T015846_012284_01319D_1D95	12284	137	111	2016-07-24T01:58:46Z	34.782	-119.6821
S1A_IW_SLC__1SDV_20160724T015843_20160724T015910_012284_01319D_9D50	12284	137	116	2016-07-24T01:59:10Z	36.2937	-120.0129
S1A_IW_SLC__1SDV_20160724T015908_20160724T015934_012284_01319D_F4F4	12284	137	121	2016-07-24T01:59:34Z	37.7613	-120.3445
S1A_IW_SLC__1SSV_20160805T015820_20160805T015846_012459_013772_EBB0	12459	137	111	2016-08-05T01:58:46Z	34.5299	-119.7976
S1A_IW_SLC__1SSV_20160805T015844_20160805T015911_012459_013772_3FD9	12459	137	116	2016-08-05T01:59:11Z	36.0394	-120.1243
S1A_IW_SLC__1SSV_20160805T015909_20160805T015936_012459_013772_7228	12459	137	121	2016-08-05T01:59:36Z	37.5483	-120.4558
S1A_IW_SLC__1SDV_20160817T015820_20160817T015847_012634_013D31_5181	12634	137	111	2016-08-17T01:58:47Z	34.7994	-119.6901
S1A_IW_SLC__1SDV_20160817T015845_20160817T015912_012634_013D31_4718	12634	137	116	2016-08-17T01:59:12Z	36.0394	-120.1241
S1A_IW_SLC__1SDV_20160817T015910_20160817T015936_012634_013D31_5CD2	12634	137	121	2016-08-17T01:59:36Z	37.4293	-120.4297
S1A_IW_SLC__1SDV_20160829T015757_20160829T015827_012809_014324_CD00	12809	137	107	2016-08-29T01:58:27Z	33.5042	-119.3872
S1A_IW_SLC__1SDV_20160829T015825_20160829T015853_012809_014324_12B9	12809	137	113	2016-08-29T01:58:53Z	34.8524	-119.8668
S1A_IW_SLC__1SDV_20160829T015851_20160829T015918_012809_014324_2FF9	12809	137	118	2016-08-29T01:59:18Z	36.3618	-120.1945
S1A_IW_SLC__1SDV_20160829T015916_20160829T015943_012809_014324_3A8A	12809	137	123	2016-08-29T01:59:43Z	37.8706	-120.5271
S1A_IW_SLC__1SDV_20160910T015821_20160910T015848_012984_0148C8_C481	12984	137	112	2016-09-10T01:58:48Z	34.53	-119.7981
S1A_IW_SLC__1SDV_20160910T015846_20160910T015913_012984_0148C8_EDE0	12984	137	117	2016-09-10T01:59:13Z	36.0394	-120.1249
S1A_IW_SLC__1SDV_20160910T015911_20160910T015937_012984_0148C8_0D2B	12984	137	122	2016-09-10T01:59:37Z	37.4294	-120.4305

Sacramento Valley (descending path 42)

Granule Name	Absolute Orbit	Path Number	Frame Number	Acquisition Date	Center Lat	Center Lon
S1A_IW_SLC__1SSV_20150301T140703_20150301T140731_004839_00605B_6C1B	4839	42	463	2015-03-01T14:07:31Z	38.6358	-120.9004
S1A_IW_SLC__1SSV_20150301T140729_20150301T140756_004839_00605B_5ECD	4839	42	468	2015-03-01T14:07:56Z	36.8651	-121.1015
S1A_IW_SLC__1SSV_20150325T140704_20150325T140731_005189_0068C0_4F8D	5189	42	463	2015-03-25T14:07:31Z	38.3731	-120.7658
S1A_IW_SLC__1SSV_20150325T140729_20150325T140756_005189_0068C0_2D18	5189	42	468	2015-03-25T14:07:56Z	36.8644	-121.1001
S1A_IW_SLC__1SSV_20150418T140705_20150418T140732_005539_00714E_BC23	5539	42	463	2015-04-18T14:07:32Z	38.3519	-120.7727
S1A_IW_SLC__1SSV_20150418T140730_20150418T140757_005539_00714E_D319	5539	42	468	2015-04-18T14:07:57Z	36.8432	-121.1069
S1A_IW_SLC__1SSV_20150512T140706_20150512T140733_005889_007958_9A43	5889	42	464	2015-05-12T14:07:33Z	38.3523	-120.7717
S1A_IW_SLC__1SSV_20150512T140731_20150512T140758_005889_007958_BC28	5889	42	469	2015-05-12T14:07:58Z	36.8436	-121.1059

S1A_IW_SLC__1SSV_20150605T140708_20150605T140735_006239_008284_8D27	6239	42	464	2015-06-05T14:07:35Z	38.352	-120.7734
S1A_IW_SLC__1SSV_20150605T140733_20150605T140800_006239_008284_8A98	6239	42	469	2015-06-05T14:08:00Z	36.8434	-121.1076
S1A_IW_SLC__1SSV_20150629T140710_20150629T140737_006589_008C6D_76A1	6589	42	464	2015-06-29T14:07:37Z	38.352	-120.7742
S1A_IW_SLC__1SSV_20150629T140735_20150629T140802_006589_008C6D_9A6F	6589	42	469	2015-06-29T14:08:02Z	36.8433	-121.1084
S1A_IW_SLC__1SSV_20150723T140710_20150723T140737_006939_00963C_DABF	6939	42	464	2015-07-23T14:07:37Z	38.3517	-120.7686
S1A_IW_SLC__1SSV_20150723T140735_20150723T140802_006939_00963C_23AE	6939	42	469	2015-07-23T14:08:02Z	36.8431	-121.1028
S1A_IW_SLC__1SSV_20150816T140711_20150816T140738_007289_009FE6_9592	7289	42	465	2015-08-16T14:07:38Z	38.352	-120.7687
S1A_IW_SLC__1SSV_20150816T140736_20150816T140803_007289_009FE6_77E1	7289	42	470	2015-08-16T14:08:03Z	36.8433	-121.1029
S1A_IW_SLC__1SSV_20150909T140712_20150909T140739_007639_00A972_5D14	7639	42	464	2015-09-09T14:07:39Z	38.3517	-120.7685
S1A_IW_SLC__1SSV_20150909T140737_20150909T140804_007639_00A972_DFD3	7639	42	470	2015-09-09T14:08:04Z	36.843	-121.1028
S1A_IW_SLC__1SSV_20151003T140713_20151003T140740_007989_00B2CA_EC3E	7989	42	464	2015-10-03T14:07:40Z	38.3518	-120.7685
S1A_IW_SLC__1SSV_20151003T140738_20151003T140805_007989_00B2CA_D9E2	7989	42	470	2015-10-03T14:08:05Z	37.111	-121.2135
S1A_IW_SLC__1SSV_20151027T140713_20151027T140740_008339_00BC45_46E2	8339	42	465	2015-10-27T14:07:40Z	38.352	-120.7695
S1A_IW_SLC__1SSV_20151027T140738_20151027T140805_008339_00BC45_9840	8339	42	470	2015-10-27T14:08:05Z	36.8433	-121.1037
S1A_IW_SLC__1SSV_20151120T140707_20151120T140734_008689_00C5C0_9D95	8689	42	463	2015-11-20T14:07:34Z	38.6852	-120.6944
S1A_IW_SLC__1SSV_20151120T140732_20151120T140759_008689_00C5C0_C157	8689	42	468	2015-11-20T14:07:59Z	37.1766	-121.0299
S1A_IW_SLC__1SSV_20151214T140706_20151214T140733_009039_00CF82_225D	9039	42	463	2015-12-14T14:07:33Z	38.6851	-120.696
S1A_IW_SLC__1SSV_20151214T140731_20151214T140758_009039_00CF82_8D56	9039	42	469	2015-12-14T14:07:58Z	37.1766	-121.0314
S1A_IW_SLC__1SSV_20160107T140705_20160107T140732_009389_00D977_A30A	9389	42	463	2016-01-07T14:07:32Z	38.6852	-120.6954
S1A_IW_SLC__1SSV_20160107T140730_20160107T140757_009389_00D977_B5FE	9389	42	468	2016-01-07T14:07:57Z	37.1766	-121.0308
S1A_IW_SLC__1SSV_20160131T140705_20160131T140732_009739_00E3A3_94F3	9739	42	463	2016-01-31T14:07:32Z	38.6851	-120.6948
S1A_IW_SLC__1SSV_20160131T140729_20160131T140756_009739_00E3A3_C165	9739	42	468	2016-01-31T14:07:56Z	37.1765	-121.0302
S1A_IW_SLC__1SSV_20160224T140704_20160224T140731_010089_00EDD9_285E	10089	42	462	2016-02-24T14:07:31Z	38.685	-120.6959
S1A_IW_SLC__1SSV_20160224T140729_20160224T140756_010089_00EDD9_4DA7	10089	42	467	2016-02-24T14:07:56Z	37.1765	-121.0314
S1A_IW_SLC__1SSV_20160319T140705_20160319T140732_010439_00F7BD_A420	10439	42	463	2016-03-19T14:07:32Z	38.6849	-120.6957
S1A_IW_SLC__1SSV_20160319T140730_20160319T140757_010439_00F7BD_B167	10439	42	468	2016-03-19T14:07:57Z	37.1763	-121.0311
S1A_IW_SLC__1SSV_20160412T140706_20160412T140733_010789_0101FE_552B	10789	42	463	2016-04-12T14:07:33Z	38.6847	-120.6951
S1A_IW_SLC__1SSV_20160412T140730_20160412T140757_010789_0101FE_CE65	10789	42	468	2016-04-12T14:07:57Z	37.1762	-121.0306
S1A_IW_SLC__1SSV_20160506T140707_20160506T140734_011139_010CD3_A1C7	11139	42	463	2016-05-06T14:07:34Z	38.6849	-120.6964
S1A_IW_SLC__1SSV_20160506T140731_20160506T140758_011139_010CD3_620C	11139	42	468	2016-05-06T14:07:58Z	37.1764	-121.0318
S1A_IW_SLC__1SSV_20160530T140708_20160530T140735_011489_011835_D5D7	11489	42	464	2016-05-30T14:07:35Z	38.6847	-120.6958
S1A_IW_SLC__1SSV_20160530T140733_20160530T140800_011489_011835_92CA	11489	42	468	2016-05-30T14:08:00Z	37.1761	-121.0313
S1A_IW_SLC__1SSV_20160810T140712_20160810T140739_012539_013A18_4411	12539	42	465	2016-08-10T14:07:39Z	38.6846	-120.6951
S1A_IW_SLC__1SSV_20160810T140737_20160810T140804_012539_013A18_F2A6	12539	42	470	2016-08-10T14:08:04Z	37.176	-121.0305

Central Coast (ascending path 137)

Granule Name	Absolute Orbit	Path Number	Frame Number	Acquisition Date	Center Lat	Center Lon
S1A_IW_SLC__1SSV_20150507T015751_20150507T015821_005809_007783_37A3	5809	137	105	2015-05-07T01:58:21Z	33.8354	-119.4634
S1A_IW_SLC__1SSV_20150531T015747_20150531T015814_006159_008023_F632	6159	137	105	2015-05-31T01:58:14Z	33.1865	-119.5128
S1A_IW_SLC__1SSV_20150531T015812_20150531T015840_006159_008023_7D81	6159	137	110	2015-05-31T01:58:40Z	34.6964	-119.8358
S1A_IW_SLC__1SDV_20150612T015747_20150612T015815_006334_008542_D264	6334	137	105	2015-06-12T01:58:15Z	33.1865	-119.5127
S1A_IW_SLC__1SDV_20150612T015812_20150612T015840_006334_008542_4F8E	6334	137	110	2015-06-12T01:58:40Z	34.6964	-119.8357
S1A_IW_SLC__1SSV_20150624T015748_20150624T015815_006509_008A40_44FD	6509	137	105	2015-06-24T01:58:15Z	33.1855	-119.5128
S1A_IW_SLC__1SSV_20150624T015813_20150624T015841_006509_008A40_161E	6509	137	110	2015-06-24T01:58:41Z	34.9397	-119.7041
S1A_IW_SLC__1SSV_20150718T015749_20150718T015816_006859_0093FC_2083	6859	137	104	2015-07-18T01:58:16Z	33.1866	-119.5076
S1A_IW_SLC__1SSV_20150718T015813_20150718T015841_006859_0093FC_8C4B	6859	137	110	2015-07-18T01:58:41Z	34.6965	-119.8306
S1A_IW_SLC__1SDV_20150730T015749_20150730T015816_007034_0098F3_8127	7034	137	105	2015-07-30T01:58:16Z	33.1865	-119.5076
S1A_IW_SLC__1SDV_20150730T015814_20150730T015842_007034_0098F3_18BF	7034	137	110	2015-07-30T01:58:42Z	34.6964	-119.8306
S1A_IW_SLC__1SSV_20150811T015750_20150811T015817_007209_009DB6_EA1C	7209	137	105	2015-08-11T01:58:17Z	33.187	-119.5084
S1A_IW_SLC__1SSV_20150811T015815_20150811T015843_007209_009DB6_2417	7209	137	110	2015-08-11T01:58:43Z	34.6969	-119.8314
S1A_IW_SLC__1SDV_20150823T015751_20150823T015818_007384_00A274_4A84	7384	137	105	2015-08-23T01:58:18Z	33.1867	-119.5091
S1A_IW_SLC__1SDV_20150823T015816_20150823T015843_007384_00A274_0FEE	7384	137	110	2015-08-23T01:58:43Z	34.6966	-119.8321
S1A_IW_SLC__1SSV_20150904T015751_20150904T015818_007559_00A743_C6AA	7559	137	106	2015-09-04T01:58:18Z	33.1867	-119.5087
S1A_IW_SLC__1SSV_20150904T015816_20150904T015844_007559_00A743_9DCE	7559	137	110	2015-09-04T01:58:44Z	34.6965	-119.8317
S1A_IW_SLC__1SDV_20150916T015751_20150916T015818_007734_00ABED_C847	7734	137	106	2015-09-16T01:58:18Z	33.1867	-119.5079
S1A_IW_SLC__1SDV_20150916T015816_20150916T015844_007734_00ABED_EB4C	7734	137	111	2015-09-16T01:58:44Z	34.6966	-119.8308
S1A_IW_SLC__1SSV_20150928T015752_20150928T015819_007909_00B0A5_2432	7909	137	106	2015-09-28T01:58:19Z	33.1869	-119.5078
S1A_IW_SLC__1SSV_20150928T015817_20150928T015844_007909_00B0A5_7CD3	7909	137	111	2015-09-28T01:58:44Z	34.6967	-119.8308
S1A_IW_SLC__1SDV_20151010T015752_20151010T015819_008084_00B54A_B0A7	8084	137	106	2015-10-10T01:58:19Z	33.1867	-119.5082
S1A_IW_SLC__1SDV_20151010T015817_20151010T015845_008084_00B54A_0E64	8084	137	110	2015-10-10T01:58:45Z	34.6965	-119.8312
S1A_IW_SLC__1SDV_20151103T015752_20151103T015819_008434_00BEB3_C649	8434	137	105	2015-11-03T01:58:19Z	33.1868	-119.5092
S1A_IW_SLC__1SDV_20151103T015817_20151103T015844_008434_00BEB3_0D17	8434	137	110	2015-11-03T01:58:44Z	34.6966	-119.8322
S1A_IW_SLC__1SSV_20151115T015746_20151115T015813_008609_00C380_8D75	8609	137	105	2015-11-15T01:58:13Z	32.8535	-119.438
S1A_IW_SLC__1SSV_20151115T015811_20151115T015839_008609_00C380_50F6	8609	137	109	2015-11-15T01:58:39Z	34.3634	-119.7601

S1A_IW_SLC__1SDV_20151127T015746_20151127T015814_008784_00C867_08C7	8784	137	105	2015-11-27T01:58:14Z	32.8534	-119.4371
S1A_IW_SLC__1SDV_20151127T015812_20151127T015838_008784_00C867_18B9	8784	137	110	2015-11-27T01:58:38Z	34.3633	-119.7591
S1A_IW_SLC__1SDV_20151221T015745_20151221T015813_009134_00D232_98B0	9134	137	104	2015-12-21T01:58:13Z	32.8532	-119.4378
S1A_IW_SLC__1SDV_20151221T015811_20151221T015838_009134_00D232_20F1	9134	137	109	2015-12-21T01:58:38Z	34.3631	-119.7599
S1A_IW_SLC__1SDV_20160114T015744_20160114T015812_009484_00DC2E_61EC	9484	137	104	2016-01-14T01:58:12Z	32.8533	-119.4378
S1A_IW_SLC__1SDV_20160114T015810_20160114T015837_009484_00DC2E_A7B7	9484	137	109	2016-01-14T01:58:37Z	34.3633	-119.7599
S1A_IW_SLC__1SSV_20160126T015744_20160126T015811_009659_00E14D_B0DD	9659	137	104	2016-01-26T01:58:11Z	32.8533	-119.4374
S1A_IW_SLC__1SSV_20160126T015809_20160126T015836_009659_00E14D_5498	9659	137	108	2016-01-26T01:58:36Z	34.3633	-119.7595
S1A_IW_SLC__1SDV_20160207T015744_20160207T015811_009834_00E65A_1651	9834	137	103	2016-02-07T01:58:11Z	32.8532	-119.4379
S1A_IW_SLC__1SDV_20160207T015809_20160207T015836_009834_00E65A_9D60	9834	137	109	2016-02-07T01:58:36Z	34.3632	-119.76
S1A_IW_SLC__1SSV_20160219T015743_20160219T015811_010009_00EB80_7305	10009	137	104	2016-02-19T01:58:11Z	32.8532	-119.4384
S1A_IW_SLC__1SSV_20160219T015809_20160219T015836_010009_00EB80_E840	10009	137	109	2016-02-19T01:58:36Z	34.3633	-119.7605
S1A_IW_SLC__1SDV_20160302T015744_20160302T015811_010184_00F077_83F4	10184	137	104	2016-03-02T01:58:11Z	32.8532	-119.4394
S1A_IW_SLC__1SDV_20160302T015809_20160302T015836_010184_00F077_C0AC	10184	137	108	2016-03-02T01:58:36Z	34.3632	-119.7616
S1A_IW_SLC__1SDV_20160314T015749_20160314T015819_010359_00F590_0DE1	10359	137	105	2016-03-14T01:58:19Z	33.4809	-119.3754
S1A_IW_SLC__1SDV_20160314T015817_20160314T015845_010359_00F590_5287	10359	137	110	2016-03-14T01:58:45Z	34.8522	-119.8666
S1A_IW_SLC__1SDV_20160326T015744_20160326T015812_010534_00FA6A_37A6	10534	137	104	2016-03-26T01:58:12Z	32.8532	-119.4392
S1A_IW_SLC__1SDV_20160326T015810_20160326T015837_010534_00FA6A_4120	10534	137	109	2016-03-26T01:58:37Z	34.3631	-119.7613
S1A_IW_SLC__1SSV_20160407T015744_20160407T015812_010709_00FF8A_CD45	10709	137	104	2016-04-07T01:58:12Z	32.8532	-119.4393
S1A_IW_SLC__1SSV_20160407T015810_20160407T015837_010709_00FF8A_150F	10709	137	109	2016-04-07T01:58:37Z	34.3632	-119.7614
S1A_IW_SLC__1SDV_20160419T015745_20160419T015813_010884_0104D5_F256	10884	137	104	2016-04-19T01:58:13Z	32.8535	-119.4392
S1A_IW_SLC__1SDV_20160419T015811_20160419T015838_010884_0104D5_C208	10884	137	109	2016-04-19T01:58:38Z	34.3635	-119.7613
S1A_IW_SLC__1SSV_20160501T015745_20160501T015813_011059_010A54_F82D	11059	137	105	2016-05-01T01:58:13Z	32.8531	-119.4395
S1A_IW_SLC__1SSV_20160501T015811_20160501T015838_011059_010A54_2DAA	11059	137	110	2016-05-01T01:58:38Z	34.3632	-119.7616
S1A_IW_SLC__1SDV_20160513T015815_20160513T015842_011234_010FDE_B126	11234	137	110	2016-05-13T01:58:42Z	34.5297	-119.7981
S1A_IW_SLC__1SDV_20160513T015749_20160513T015817_011234_010FDE_1832	11234	137	105	2016-05-13T01:58:17Z	33.0198	-119.4755
S1A_IW_SLC__1SSV_20160525T015749_20160525T015817_011409_01159A_5B0C	11409	137	105	2016-05-25T01:58:17Z	33.0198	-119.4742
S1A_IW_SLC__1SSV_20160525T015815_20160525T015842_011409_01159A_A7C0	11409	137	110	2016-05-25T01:58:42Z	34.5298	-119.7968
S1A_IW_SLC__1SDV_20160606T015750_20160606T015818_011584_011B33_1C2D	11584	137	106	2016-06-06T01:58:18Z	33.2748	-119.3629
S1A_IW_SLC__1SDV_20160606T015816_20160606T015843_011584_011B33_10B8	11584	137	111	2016-06-06T01:58:43Z	34.7982	-119.69
S1A_IW_SLC__1SDV_20160630T015752_20160630T015819_011934_012632_DD4A	11934	137	106	2016-06-30T01:58:19Z	33.0199	-119.4754
S1A_IW_SLC__1SDV_20160630T015817_20160630T015844_011934_012632_783B	11934	137	111	2016-06-30T01:58:44Z	34.5299	-119.7979
S1A_IW_SLC__1SDV_20160724T015753_20160724T015821_012284_01319D_CFD1	12284	137	106	2016-07-24T01:58:21Z	33.0199	-119.4747
S1A_IW_SLC__1SDV_20160724T015819_20160724T015846_012284_01319D_1D95	12284	137	111	2016-07-24T01:58:46Z	34.782	-119.6822
S1A_IW_SLC__1SSV_20160805T015754_20160805T015822_012459_013772_729B	12459	137	106	2016-08-05T01:58:22Z	33.02	-119.475
S1A_IW_SLC__1SSV_20160805T015820_20160805T015846_012459_013772_EBB0	12459	137	111	2016-08-05T01:58:46Z	34.5299	-119.7976
S1A_IW_SLC__1SDV_20160817T015754_20160817T015822_012634_013D31_E7CB	12634	137	106	2016-08-17T01:58:22Z	33.02	-119.4748
S1A_IW_SLC__1SDV_20160817T015820_20160817T015847_012634_013D31_5181	12634	137	111	2016-08-17T01:58:47Z	34.7994	-119.6901

UAVSAR

The two UAVSAR flight lines used for evaluating subsidence of the California Aqueduct were line ID CValle_13300 (southern section) and line ID Snjoaq_14511 (northern section). Table A2 shows the flight dates, UAVSAR flight IDs, and temporal baselines for lines 13300 and 14511. Each acquisition was used in at least three interferograms to provide sufficient redundancy to eliminate systematic effects from atmospheric variation and aircraft motion artifacts.

Table A2. UAVSAR line ID, flight ID, and acquisition date of the data used for evaluating subsidence of the California Aqueduct during the 2014 drought.

UAVSAR Line ID 14511			**UAVSAR Line ID 13300**		
Acq. No.	**Flight ID**	**Date of acquisition**	**Acq. No.**	**Flight ID**	**Date of acquisition**
1	13129	7/19/2013	1	14033	4/2/2014
2	13165	10/31/2013	2	14062	5/15/2014
3	14005	1/17/2014	3	14086	6/16/2014
4	14019	2/12/2014	4	14112	8/14/2014
5	14033	4/2/2014	5	14140	10/6/2014
6	14068	5/29/2014	6	14166	11/13/2014
7	14086	6/16/2014	7	15002	1/7/2015
8	14112	8/14/2014	8	15053	4/27/2015
9	14140	10/6/2014	9	15149	10/7/2015
10	14166	11/13/2014	10	16003	2/18/2016
11	15002	1/7/2015	11	16056	6/14/2016
12	15017	3/10/2015			
13	15053	4/27/2015			
14	15056	5/16/2015			
15	16003	2/18/2016			
16	16056	6/14/2016			

UAVSAR uncertainties

Figures A1 and A2 show the uncertainties associated with the vertical displacement (subsidence/uplift) measurements. These uncertainties cover random errors, but do not include systematic errors, i.e., systematic shifts that affect all interferograms, for example, persistent water vapor within mountain valleys, were it present in all images, would not be included in the error estimation.

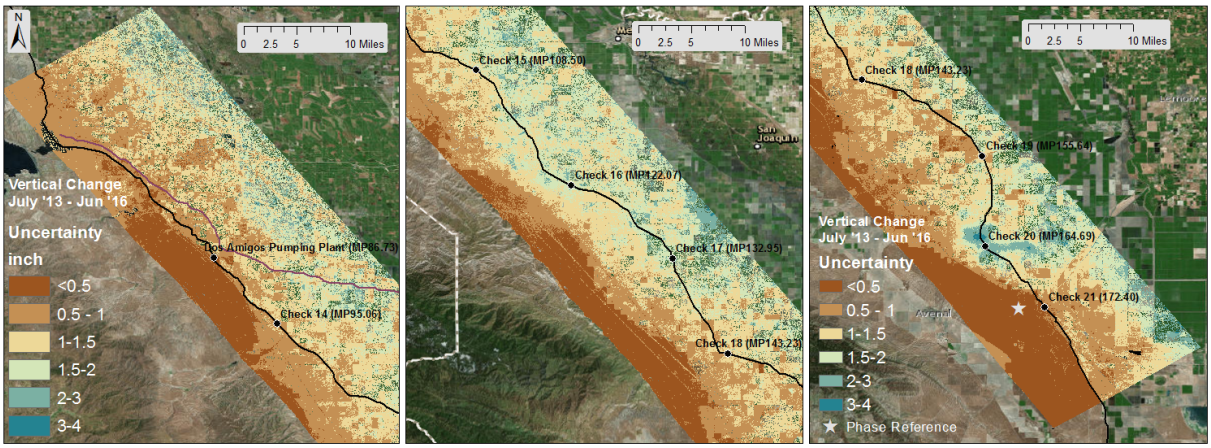

Service Layer Credits: Source: Esri, DigitalGlobe, GeoEye, i-cubed, Earthstar Geographics, CNES/Airbus DS, USDA, USGS, AEX, Getmapping, Aerogrid, IGN, IGP, swisstopo, and the GIS User Community

Figure A1. Uncertainty in the vertical movement derived from UAVSAR line ID 14511, covering the section of the California Aqueduct within the area overseen by the San Luis Field Division. The swath is split into three images with the northern/center/southern part of the line plotted at left/center/right.

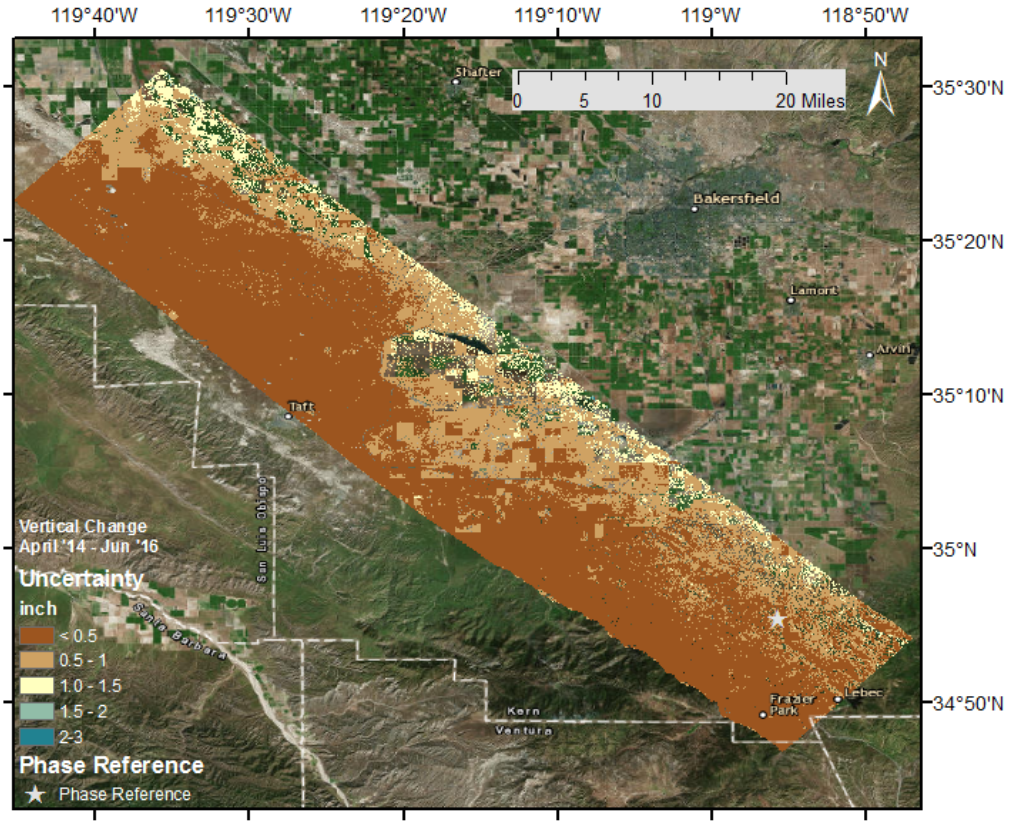

Service Layer Credits: Source: Esri, DigitalGlobe, GeoEye, i-cubed, Earthstar Geographics, CNES/Airbus DS, USDA, USGS, AEX, Getmapping, Aerogrid, IGN, IGP, swisstopo, and the GIS User Community
Esri, HERE, DeLorme, TomTom, MapmyIndia, © OpenStreetMap contributors, and the GIS user community

Figure A2. Uncertainty in the subsidence derived from UAVSAR line ID 13300, covering the southern section of the California Aqueduct within the area overseen by the San Joaquin Field Division.